ACS OMEGA

Open Access

http://pubs.acs.org/journal/acsodf

Article

Formulation of Folate Receptor-Targeted Silibinin-Loaded Inhalable Chitosan Nanoparticles by the QbD Approach for Lung Cancer Targeted Delivery

Priya Patel,* Mihir Raval, Vishal Airao, Nemat Ali,* Gamal A. Shazly, Rehan Khan, and Bhupendra Prajapati

Cite This: *ACS Omega* 2024, 9, 10353−10370

Read Online

ACCESS | Metrics & More | Article Recommendations

ABSTRACT: ***Aim***: Targeted delivery of chemotherapeutics by functionalized nanoparticles exhibits a wonderful prospect for cancer treatment. The main objective of this research was to develop folate receptor-targeted silibinin (SB)-loaded inhalable polymeric nanoparticles (FA-CS-SB-NPs) for the treatment of lung cancer. ***Method***: The qbD approach was implemented to prepare SB-loaded nanoparticles. Folic acid was conjugated by electrostatic conjugation in an optimized batch. The therapeutic potentials of formulations were determined using a lung cancer cell-bearing rat model. ***Result***: Optimized formulation exhibited a spherical surface with a mean particle size of 275 ± 1.20 nm, a PDI of 0.234 ± 0.07, a ζ-potential of 32.50 ± 0.21, an entrapment efficiency of 75.52 ± 0.87%, and a CDR of 63.25 ± 1.21% at 48 h. Aerodynamic behaviors such as the mass median aerodynamic diameter (MMAD) and geometric size distribution (GSD) were found to be 2.75 ± 1.02 and 3.15 ± 0.88 μm, respectively. After 24 h of incubation with FA-CS-SB-NPs, the IC50 value was found to be 24.5 g/mL. FA-SB-CS-NPs maintained a significantly higher deposition of SB in lung tissues. ***Conclusions***: Thus, the noninvasive nature and target specificity of FA-CS-SB-NPs pave the way for pulmonary delivery for treating lung cancer.

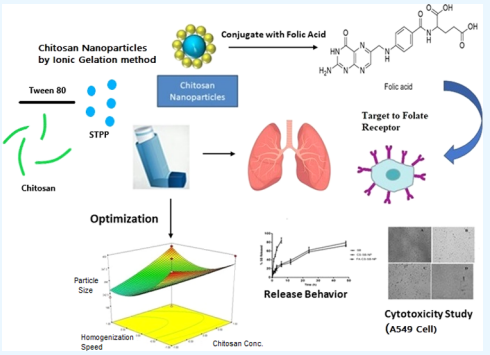

INTRODUCTION

Lung cancer is one of the most common cancers, and it plays an important role, with a higher mortality rate in both primary and metastatic neoplasia. The World Health Organization categorizes lung cancer into four primary types: adenocarcinoma, large-cell carcinoma, squamous-cell carcinoma, and small-cell carcinoma. Photodynamic therapy, chemotherapy, surgery, and target-specific therapy are all options for lung cancer treatment.[1]

The main component of the silymarin extract is silibinin, flavonolignan that can be found in the seeds and fruits of Silybum marianum.[2] This phytoconstituent has been shown to have antioxidant, cardioprotective, anticancer, anti-inflammatory, and neuroprotective properties. Silibinin has been approved by the USFDA as safe with no significant side effects. According to the researcher's analysis of the literature, silibinin was utilized in the treatment of different types of cancers, including colon cancer, lung cancer, skin cancer, cervical cancer, and ovarian cancer.[3] Silibinin is rapidly absorbed after oral administration, with a tmax of 2−4 h and a half-life of 6 h. Conventional silibinin has a low oral rate of absorption of 23−47%, resulting in low bioavailability. Low water solubility, less penetration into gut epithelial cells, metabolism in the liver, and rapid systemic clearance may all contribute to the drug's low bioavailability.[4,5] Nanomedicine has evolved dramatically in cancer therapy over the past decade, and a substantial quantity of nanoscale drug carriers have been built to carry chemotherapeutic medications to increase bioavailability and tissue delivery with the main goal of improving the therapeutic index.[6] The nanoparticulate drug delivery technology embraces tremendous promise for successfully enhancing the therapeutic effectiveness of multiple anticancer drug molecules. Recent nanotechnology expansion has produced a variety of nanomaterials suitable to treat lung cancer.[6] Nanoparticles, renowned for their biocompatibility, serve as optimal carriers for in vivo drug delivery to cancer cells. Among them, chitosan NPs (CSNPs) stand out with exceptional attributes, showcasing controlled release behavior. The unique advantages of chitosan NPs make them a promising technology for precise and effective drug delivery

Received: October 11, 2023
Revised: January 25, 2024
Accepted: February 7, 2024
Published: February 24, 2024

in the fight against cancer.[7,8] CSNPs are susceptible to modification by other ligands, such as folates, epidermal growth receptors, and polypeptides, due to their primary amino acids.[9] Hence to improve the modification of CSNPs with ligands that are specific for receptors on tumor cells, which can lead to the specificity of drug delivery to tumor cells.

Improving CSNPs' targeting efficacy involves linking them to specific ligands, such as antibodies or low-molecular-weight compounds like folate, through chemical or biological conjugation. This enhancement strategy aims to optimize the precision and efficiency of CSNP interactions with target entities. The folate is a well-studied ligand due to its stability, minimal immunogenicity, and low cost. Furthermore, human cancer cells, including A549 cells, show higher levels of folate receptors (FRs) than normal cells.[10]

Folate is a well-known tumor-targeting moiety and it is frequently conjugated with NPs because of its capacity to form a unique bond with FRs.[11] The c-carboxyl derivative component of conjugated folates is covalently bonded, which explains the high affinity of folate ligands. The uptake of folate-conjugated substances by FRs has comparable kinetics to that of free folate.[12] FRs are promising therapeutic targets that are influenced by a variety of cancers. Folate is thought to act as a targeting ligand for anticancer drugs, limiting undesired attacks on healthy tissues. Folate enters targeted tumor cells via the endocytosis process with the help of cellular receptors, enhancing cellular uptake.[13] To summarize, folate-conjugated nanoparticles are suitable polymeric carriers for targeted medication delivery to malignancies.

A new approach to nanotechnology has arisen in the recent decade, with the purpose of focusing on lung disorders such as cancer. The idea is to combine pharmaceutical delivery using nanotechnology with an inhalational delivery device. This method has sparked research into the lung's potential utility as a doorway for pharmaceutical entrance. Because of their vast surface area for absorption (100 m) and relatively thin absorption membrane (0.1−0.2 m), the lungs are a well-organized channel for medicines into the bloodstream. Furthermore, the lungs have lower local metabolic activity than the oral route, and the inhalation route is less sensitive to first-pass metabolism.[14,15] Chemotherapy inhalation has been confirmed to be beneficial for treating lung cancer. When compared to parenteral delivery, inhalation can modify the biodistribution of medications and boost the accumulation of their noticeably higher fraction in the lungs. Inhalation also helps to limit the systemic distribution of anticancer drugs, which reduces their associated toxicity.[16,17] As a result, targeted inhalational NP administration to the lungs is a promising field of cancer nanotechnology research that many formulation scientists, oncologists, and biomedical researchers are interested in.

The concept of quality by design (QbD) is becoming widely accepted in the pharmaceutical development industry due to its overall productivity in optimizing an appropriate experimental design space. Pharmaceutical quality by design (QbD) is an organized development methodology that begins with predetermined objectives and places a strong emphasis on understanding and controlling processes and products using applied science and risk management for the nanoparticles developed for the inhalation route.[18] The use of the quality by design (QbD) methodology has resulted in the establishment of standardized, formulation-driven procedures for getting the optimum product. Successful commercialization of nanosized formulations containing anticancer medicines might be possible if scaling-up challenges are properly addressed.[19]

DoE studies, such as Plackett−Burman (PB) and Box−Behnken designs, must be performed on important parameters based on risk assessment of process and formulation factors; specific ranges for critical parameters should be established within specified ranges to obtain the desired outcome (degree of substitution (DS)).[20,21] Videira et al. proved that a paclitaxel-loaded lipid nanocarrier was found to be more efficacious compared to IV therapy.[22] Tomoda et al. claimed that by spray-dried PLGA NP drug concentration in the lungs was found to be greater after intravenous delivery of the free drug.[23] Roa et al. confirmed that Inhalable effervescent DOX NPs were found to be an effective treatment for lung cancer in their investigation.[24]

The aim of the current research was to develop folic acid-conjugated silibinin-loaded CSNPs and to assess their synergistic anticancer effectiveness in a lung cancer mouse model. Moreover, in this study, we explored the antiproliferative effects on A549 cells, bioavailability, pharmacokinetics, and tissue distribution study. This platform significantly increased drug delivery to the tumor while also producing great efficacy. The drug carrier folic acid-linked nanoparticles could be effective in treating lung cancer. In this case, drug delivery that targets receptors has the potential to be highly beneficial in correcting the poor pharmacokinetics of silibinin and enhancing therapeutic outcomes in patients with advanced lung cancer.

MATERIALS AND METHODS

Materials. Silibinin was procured from Sigma-Aldrich, Mumbai (India). Chitosan (CS) (M.W 120−350 kDa, degree of deacetylation: 95%) was gifted by Cognis Gmbh Pvt. Ltd. Germany as a polymer. Sodium tripolyphosphate (STPP) as a cross-linking agent, Tween 80 as a surfactant, 4-(methylnitrosamino)-1-(3-pyridyl)-1-butanone (NNK) as a lung cancer inducer, and folic acid as an active targeting agent were purchased from Sigma-Aldrich, Mumbai (India). All other excipients and solvents were of pharmaceutical and analytical grade. Double distilled water was used throughout the study.

Method. Preparation of CSNPs was accomplished using an ionic gelation technique.[23] Chitosan was dissolved in an aqueous solution of acetic acid (0.02% v/v) to obtain a 0.5 mg/mL chitosan solution. Silibinin and Tween 80 were dispersed in the above solution with constant stirring. Cross-linker STPP was dissolved in distilled water at a concentration of 0.5 mg/mL. An STPP aqueous solution was added dropwise using a syringe needle (0.22 μm, Millipore) into the above chitosan solution containing SB with continuous stirring at different speeds by a high-speed homogenizer (IKA T25 Digital S22 Homogenizer, India). The stirring was continued for a specific amount of time. The resulting nanosuspension was centrifuged at 8000 rpm for 30 min before being washed with distilled water (Remi Laboratory Centrifuge, R-4CDX). Because the centrifugation process generates a lot of heat, the temperature was kept at −4 °C to keep the nanoparticles stable. The supernatant liquid was removed, and the settling nanoparticles were redispersed in a phosphate-buffered solution pH 7.4 and ultrasonically disaggregated for 5 min.[25]

Freeze-Drying of Chitosan NPs. Two milliliters of the nanoparticle suspension was placed in glass vials with rubber stoppers for lyophilization. The freeze-dryer (LSFD1SU, Delvac Pumps Pvt. Ltd., Chennai, India) was set at −40 °C

https://doi.org/10.1021/acsomega.3c07954
ACS Omega 2024, 9, 10353−10370

for 72 h. Detailed procedures were performed as per methods described in Patel et al.[26,27]

Defining the Quality Target Product Profile and Critical Quality Attributes. A number of patient-centered quality characteristics (QA) were found to satisfy the QTPP, including physical properties of drugs such as particle size, entrapment, and cumulative drug release after 24 h. Biopharmaceutical Performance, it is imperative to understand which of these can potentially be the critical quality attributes (CQAs) of nanoparticle formulations.[28]

Risk Assessment. A risk assessment plan was developed in order to classify probable interactions between drugs and excipients with various unit activities and to quantify the risk(s) or failure(s), if any. The Ishikawa diagram was created to structure the risk assessment process to identify the causes and components that affect the CQA of a drug.

Risk Analysis by the Placket−Burman Design (PBD). The relative effects of particle size, entrapment efficiency, and cumulative drug release after 48 h of nanoparticles were assessed using PBD as the primary screening method. On the basis of preliminary investigations, high and low values for each factor were selected. The PBD was constructed with 12 runs using Design Expert software (Trial version 12.0.0, Stat- Ease Inc.). Based on risk assessment, seven independent variables were selected. The variables with significant main impacts on the selected responses were identified using the Pareto chart and analysis of variance (ANOVA) results.[29]

Optimization Using the Box−Behnken Design. A Box−Behnken experimental design with 3 factors, 3 levels, and 15 runs was chosen for the optimization study. Particle size, encapsulation efficiency, and cumulative drug release at 48 h (CDR at 48 h) were selected as dependent variables. For predicting the optimal region, a quadratic equation generated for the variables is explained below in eq 1.

$$Y = \beta_0 + \beta_1 X_1 + \beta_2 X_2 + \beta_3 X_3 + \beta_{12} X_1 X_2 + \beta_{13} X_1 X_3 + \beta_{23} X_2 X_3 + \beta_{123} X_{123} \beta_1^2 X_1^2 + \beta_2^2 X_2^2 + \beta_3^2 X_3^2 \quad (1)$$

where Y denotes the measured response, β_0 denotes the constant, and β_1, β_2, and β_3 are the coefficients for the factors X_1, X_2, and X_3. The coefficients of interaction are β_{12}, β_{23}, β_{13}, and β_{123}, while the coefficients of the quadratic terms are β_1^2, β_2^2, and β_3^2.

All DOE statistical treatments were performed using Design Expert software (Trial ver. 12.0.0, Stat- Ease Inc.).[29,30]

Optimization of the Design Space and Validation of the Model. The polynomial equations were developed by the trial version of Design Expert Software (12.0.0) and also tested to refine the models for statistical significance. The checkpoint batches were selected within the design space and compared between the predicted and experimental results of the responses, and % error was calculated to validate the selected model by using below eq 2.[31]

$$\%\ \text{relative error} = \frac{\text{predicted value} - \text{experimental value}}{\text{predicted value}} \times 100 \quad (2)$$

Characterization and Evaluation of Prepared Nanoparticles. *Measurement of the Particle Size, ζ-Potential, and Polydispersity Index.* The physicochemical properties of nanoparticles, such as particle size, polydipsersity index (PDI), and ζ-potential of the particles, were measured on a Zetasizer-Nano ZS (ZEN3600 Malvern Zetasizer Nano series Nano-ZS, UK.) as per the method described in Patel et al.[26,32]

Measurement of Drug Entrapment Efficiency. %EE was calculated by centrifugation of the aqueous phase to determine the free drug concentration. % EE was measured as per the method described in Patel et al.[26,32] The % EE was calculated using the following eq 3.

$$\%\ \text{entrapment efficiency} = \left(\frac{\text{total amount of drug} - \text{free amount of drug}}{\text{total amount of drug}}\right) \times 100 \quad (3)$$

In Vitro Drug Release and Drug Release Kinetic Study. Modified dialysis diffusion techniques were employed to determine the drug release profile from produced polymeric nanoparticles. Drug release and release kinetics were measured as per methods described in Patel et al.[26,33,34] The produced sample was quantified using an HPLC System (Shimadzu Corporation, Japan).

Method of Conjugation of Folic Acid on Nanoparticles. Ten milligrams of folic acid was dissolved in a solution containing 2 mL of anhydrous dimethyl sulfoxide and 10 mL of a 20% w/v aqueous solution of sodium hydroxide. The resulting solution was dropped into 10 mL of a phosphate-buffered solution pH 7.4 containing 30 mg of optimized nanoparticles prepared for 30 min under stirring conditions using a laboratory magnetic stirrer at 500 rpm (Remi Instrument Pvt Ltd., Ahmedabad). The resulting solution was subjected to a high-speed homogenizer (Omni Programmable digital Homogenizer, Mumbai) at 5000 rpm for 4 h. Loading efficiency of the difference between the amount of folic acid initially added and the amount of folic acid in the supernatant was used to determine the amount of folic acid in the produced nanoparticles. To obtain powders, the collected products were washed three to four times with deionized water, centrifuged at 15,000 rpm for 15 min, and then freeze-dried (FA-CS-SB-NPs).[35]

Formulation of the Inhalable Powder. Initially, flow property was calculated for silibinin nanoparticles. The FA-CS-SB-NPs and anhydrous inhalable-grade lactose were manually mixed (1:1.5.) using the geometric dilution method to increase the flow property. The Hausner ratio, angle of repose, and Carr's index were carried out after adding inhalable-grade lactose.[36] The optimized formulation was then analyzed for particle size to see how the nanoparticles changed on being inhaled.

Determination of Mass Median Aerodynamic Property Evaluation. The mass median aerodynamic diameter (MMAD) of unconjugated nanoparticles and folic acid-conjugated nanoparticles were investigated by using an Andersen cascade impactor with eight stages (model 200-800, Thermo Fischer Scientific, MA). Procedures were performed as per the method described in Patel et al. The percent respirable fraction (RF) was calculated as mentioned below in eq 4.[26,37]

$$\%\text{RF} = \frac{\text{amount of drug deposited on stage 2 through 7}}{\text{total loaded dose}} \times 100 \quad (4)$$

Characterization of the Prepared Folic Acid-Conjugated Chitosan Nanoparticles (FA-CS-SB-NPs). *Fourier*

https://doi.org/10.1021/acsomega.3c07954
ACS Omega 2024, 9, 10353−10370

Transform Infrared (FTIR) Spectroscopy. The IR spectra of compounds such as silibinin, chitosan, and folic acid-conjugated nanoparticles were recorded using FTIR spectroscopy (CARY 630, Agilent Technologies). Spectra were recorded as per the method described in Patel et al.[26,38]

Differential Scanning Calorimetry (DSC). DSC analysis of the samples was performed on a DSC 60 (Shimadzu, Tokyo, Japan) precalibrated for temperature and heat flux accurately using indium. DSC analysis of the samples such as silibinin, chitosan, and folic acid-conjugated nanoparticles was performed as per the method described in Patel et al.[26,38]

Scanning Electron Microscopy (SEM). SEM (JEOL-JSM-6380LVERDA) was used to examine the form and surface morphology of the optimized folic acid-conjugated CSNPs. To determine the surface morphology, shape, and size of each sample, images were taken at varying magnifications in a vacuum chamber while placing the probe.[38]

Nuclear Magnetic Resonance (NMR). The NMR spectra of folic acid-conjugated CSNPs were acquired using a 500 MHz NMR spectrometer (AVANCE 500, Bruker, Rheinstetten, Germany) and a CF3COOD/D2O mixture (0.1 mL CF3COOD in 0.5 mL D2O) as a solvent. The NMR spectra of the FA-CS molecule were used to calculate the degree of substitution (DS) of folic acid to the monosaccharide residue of CS.[38]

X-ray Powder Diffraction Study. A Pananalytic diffractometer system recorded X-ray powder diffraction patterns of pure drug and folic acid-conjugated CSNPs (Xpert pro-PW 30-40/60 multipurpose diffractometer, Philips, India). The samples were inserted in a sample holder and scanned at a scan angular speed of 2θ min^{-1} from 2θ to 50θ. The diffraction patterns were collected and plotted using Xpert High Score Plus software.[39]

In Vitro Cytotoxicity Assay. In Vitro Cytotoxicity Assay Performed in A549 Cells by MTT Assay. A549 cells were cultured in an RPMI medium supplemented with 10% (v/v) fetal bovine serum and gentamycin sulfate (10 g/mL) (NCCS, Pune, Maharashtra, India). Cells were maintained at 37 °C in a 5% CO_2/95% air-humidified incubator. A549 cells were seeded in 96-well plates at a density of 10,000 viable cells per well and incubated for 24 h to allow cell adhesion. Various concentrations of prepared formulations (CS-SB-NPs and FA-CS-SB-NPs) ranging from 0.39 to 50 μg/mL and pure silibinin were added to the respective wells along with blank and untreated controls in triplicate. Plates were incubated for 24 h at 37 °C in a CO_2 incubator.[40,41] The whole procedure was performed as per the method described in Patel et al.[26] Using eq 5, the percent cell viability was computed using untreated cells as 100%. Results are expressed as the percentage of Viable cells respect to control values.

$$\text{percent cell viability} = \frac{\text{absorbance test}}{\text{absorbance control}} \times 100 \quad (5)$$

In Vivo Study. *Animals.* Sprague-Dawley rats (weight: 200−250 g) were housed in polypropylene cages under standard conditions of temperature (25 ± 10 °C), relative humidity (55 ± 10%) cycle, and ad libitum supply of standard food and filtered water. Animals were acclimatized to a 12 h light/dark period 1 week before the experiment and fasted overnight with free water to access. The Institutional Animal Ethics Committee (IAEC), Department of Pharmaceutical Sciences, Saurashtra University, Rajkot, Gujarat, India, was formed in accordance with the guidelines of the Committee for the Purpose of Control and Supervision of Experiments on Animals (CPCSEA), Government of India (Protocol approval no.: IAEC/DPS/SU/1705; dated 12th December, 2016).

NNK Lung Cancer Model. The lung cancer model was developed using the method given by Bhatnagar et al. and was modified to meet the needs of the study.[42] After 1 month, the rats were given a single high dosage (2.5 mg/kg body weight) of NNK, followed by 3 weeks of lower doses (1.5 mg/kg body weight), for a total dose of 100 mg/kg body weight. Two animals were sacrificed every month for 3 months and in the 5th month. At each month, lungs, liver, kidneys, and spleen were removed for histopathological evaluations. Blood samples from rats were collected from the tail vein, and serum was separated for further biochemical estimations to analyze the various biochemical parameters during the induction period of lung cancer. The experiments were terminated after 20 weeks. When tumor volumes grew to 100 mm^3, the tumor volume was calculated with eq 6 as follows

$$\text{tumor volume } (mm^3) = 1/4 \times \text{length} \times \text{width}^2 \quad (6)$$

Rats were randomly asssigned into three groups, namely, saline, CS-SB-NP, and FA-CS-SB-NP with 06 animals in each. Control animals were injected with saline on the same schedule. The prepared formulation (2.5 mg/kg) was given by a microspray aerosolizer through an inhalation route continued for 2 months for 3 days a week. The remaining tumor-induced rats were used for further study.

Sample Collection and Serum Preparation. After anesthesia with diethyl ether, blood was collected from the tail vein using heparinized capillary tubes. The blood was allowed to clot for 30 min at room temperature and then centrifuged for 20 min at 1200 rpm. The serum was then aliquoted and stored at −80 °C until use.

Biochemical Measurements. *Estimation of Lipid Peroxidation.* The reaction mixture contains 500 L of a 10% homogenate, 500 μL of 15% TCA, 300 μL of 25% TBA, and 300 μL of 5 N HCL in a total volume of 1.6 mL. For 15 min, the reaction mixture was immersed in boiling water at 95 °C. Finally, the tubes were placed on ice and centrifuged at 3000 rpm for 10 min. The absorbance at 512 nm of the supernatant containing thiobarbituric acid reactive substances (TBA-RS) was measured using a UV spectrophotometer.[43]

Estimation of Superoxide Dismutase Activity. The reaction mixture contained 25 μL of the homogenate, 0.2 mL of epinephrine, and 0.8 mL of carbonate buffer (pH 9.2). A UV spectrophotometer was used to detect absorbance at 295 nm. SOD activity was measured in units per milligram of the protein.[44]

Estimation of Catalase Activity. The assay combination consisted of 1.95 mL of phosphate buffer (0.05 M, pH 7.0), 1.0 mL of hydrogen peroxide (0.019 M), and 50 L of serum in a total of 2.0 mL. A UV spectrophotometer was used to record the rate of change in absorbance per minute at 240 nm.[45]

Estimation of Glutathione Reductase Activity. The assay system taken in a 3 mL quartz cuvette consisted of 1.0 mL of Tris EDTA (0.2M), 0.9 mL of EDTA (20 mM), and 20 μL of Elman's reagent. The mixture was incubated for 30 min and 100 μL of the homogenate was added. The mixture was measured at an absorbance of 412 nm by a UV−visible spectrophotometer.[46]

Histological Examinations. During the experiment, animals were sacrificed under ether anesthesia at specific time intervals and following treatment, and important organs such as the

https://doi.org/10.1021/acsomega.3c07954
ACS Omega 2024, 9, 10353−10370

lungs, liver, spleen, and kidneys of rats from each group were rapidly removed. The specimens were postfixed in buffered formalin (10% v/v) for 24 h. Tissues were sectioned (3−4 mm thick) after fixation, dried with 100% alcohol, embedded in new paraffin, and allowed to cool. Cross sections of each tissue were cut on a microtome and stained with hematoxylin and eosin (H&E). Using an Olympus BX50 Microscope System (Olympus, Japan), microphotographs were taken and the slides were examined for histopathological anomalies.[42]

Biodistribution Study. Tumor-bearing rats were used in biodistribution studies. After the tumors developed in rats, a biodistribution study was carried out. The animals were separated into three groups of six for free SB, CS-SB-NPs, and FA-CS-SB-NPs. Standard SB was supplied by the lateral vein at a dose of 3.5 mg/kg body weight. The rats were given CS-SB-NPs and FA-CS-SB-NPs (2.5 mg/kg) using a microspray aerosolizer. Animals from each group were sacrificed at specific times, such as 2, 8, 24, and 48 h. Blood samples were drawn from the ocular artery and deposited in test tubes containing a heparin solution of 10 L. The plasma was centrifuged immediately and kept at −20 °C until the assay. Organs such as the lungs, livers, and kidneys were taken. Before homogenization, organs were washed with saline and weighed. To prepare tissue samples for homogenization, 0.5 mL of plasma (or tissue homogenate) was added to 0.2 mL of a methyl testosterone methanol solution (7 g/mL) as the in-house standard for silibinin analysis. Tissue samples were then placed on ice. For 5 min, the mixture was vortexed with 3 mL of aceto acetate and then centrifuged at 3000 rpm for 10 min. After 10 min, dry samples were reconstituted with 0.4 mL of methanol and further centrifuged at 2000 rpm. HPLC was used to determine the total quantity of silibinin.[47]

The total targeting efficiency (T_e^c), targeting index (r_e^c), and relative overall targeting efficiency (R_{Te}^c) of the prepared nanoparticles were measured and compared to those of the silibinin solution in order to assess the lung-targeting characteristic of the chitosan-coated PLGA inhalable nanoparticles. The three targeting evaluation 7−9 indices are as follows.

$$r_e^c = (\mathrm{AUC})\mathrm{NP}/(\mathrm{AUC})\mathrm{sol} \tag{7}$$

$$T_e^c = (\mathrm{AUC})\mathrm{TM}/(\mathrm{AUC})I \tag{8}$$

$$R_{Te}^c = (T_c\mathrm{NP} - T_c\mathrm{Sol})/T_c\mathrm{Sol} \times 100\% \tag{9}$$

where the denomination refers to the sum total of drug exposure to all tissues, including the targeted tissue (Sol: SB-sol; NP: SB-NP).

Assessment of Antitumor Activity. After tumor induction, rats were randomly assigned into four groups: control, SB, CS-SB-NPs, and FA-CS-SB-NPs nanoparticles, each with six animals. On the same day, control animals received saline injections. Prepared CS-SB-NPs and FA-CS-SB-NPs nanoformulations were administered by a microspray aerosolizer for 2 months at a dose comparable to 2.5 mg/kg body weight of SB. At days 0, 3, 12, 18, 24, and 30, rats were frequently examined for differences in tumor size. A vernier caliper was used to determine the size of the tumor mass.[48] Tumor volumes were determined using eq 10.

$$\text{tumor volume } (\mathrm{mm}^3) = 1/4 \times \text{length} \times \text{width}^2 \tag{10}$$

Colloidal Stability. In homogenates of plasma, serum, liver, kidneys, brain, spleen, and lungs, colloidal stability was assessed. Blood was drawn from the retro-orbital sinus of anesthetized animals, and plasma and serum were separated by centrifugation at 3000 rpm for 10 min; the tissues underwent homogenization in 2 mL of pH 7.5 phosphate buffer, followed by a 10 min centrifugation at 4 °C and 10,000 rpm.[45] Before being used in a colloidal stability study, the supernatant was extracted and diluted 1:10 (v/v) with deionized water. After 2, 4, 6, 8, 12, 24, and 48 h in biological fluids, the particle size of the generated SB-loaded PCL/Pluronic F68 NP was measured.

Pharmacokinetic Study. Rats were randomly distributed in three groups (n = 6). Group I was administered with pure silibinin (3.5 mg/kg). Group II and III were administered through a microspray aerosolizer with CS-SB-NP and FA-CS-SB-NP (2.5 mg/kg). Serial blood samples were obtained from the retro-orbital plexus of rats at intervals of 2, 3, 4, 6, 8, 12, 24, and 48 h in plastic tubes containing heparinized saline, which acts as an anticoagulant. Plasma samples were obtained by centrifuging the blood at 10,000 rpm for 20 min at 40 °C and storing them at 200 °C before analysis (Centrifuge 5418R, Eppendorf AG, Germany). Drugs were extracted from rat plasma using a simple protein precipitation process and measured using HPLC analysis.[49]

High-Performance Liquid Chromatography. An HPLC System (Shimadzu Corporation, Japan) was utilized to quantify SB in prepared samples. The system was managed using a CTO-20AC column oven with an autosampler and a C18 (250 4.6 mm) agilent column. The method was found to be linear in the 5−30 μg/mL concentration range (R^2 = 0.9995; n = 3).[50]

Data Analysis. Profiles of plasma concentration (g) vs time (h) were created, and the peak plasma concentration (C_{max}) and time of occurrence (T_{max}) were directly recorded from the profiles. GraphPad Prism version 4 was used to calculate the area under the concentration−time curve (AUC_{0t}) using the linear trapezoidal method.

The mean and standard deviation of all pharmacokinetic parameters of the produced chitosan NPs and the silibinin solution were calculated (SD). Graph Pad Prism statistical analysis was used to analyze the data, which included a student's unpaired t test. The significance levels were set at <0.05, < 0.01, and <0.001.

Toxicity Experiment. Rats were randomly divided into various groups, such as the control group (n = 6), the pure SB group (n = 6), and folic acid-conjugated nanoparticles (n = 6). The experimental group was treated with SB (3.5 mg/kg) and folic acid-conjugated nanoparticles (2.5 mg/kg) daily for 2 weeks. Every day, the control group was given normal saline through the caudal vein. During this period, all rats were allowed to drink water and eat. The rats were sacrificed 2 weeks later to acquire several tissues (lungs, liver, kidneys, and spleen) for weighing.[50] The immune organ index was calculated using eq 11.

$$\text{immune organ index} = \frac{\text{weight of immune organs } (G)}{\text{body weight } (G)} \tag{11}$$

Accelerated Stability Study. According to the International Conference on Harmonization (ICH) Q1A(R2) guidelines and a previously documented approach by Chalikwar et al.,[51] the optimized batch of inhalable FA-CS-SB-NP was used to conduct accelerated stability studies. Particle size, percent EE, and percent CDR were measured after 48 h of redispersion of

https://doi.org/10.1021/acsomega.3c07954
ACS Omega 2024, 9, 10353−10370

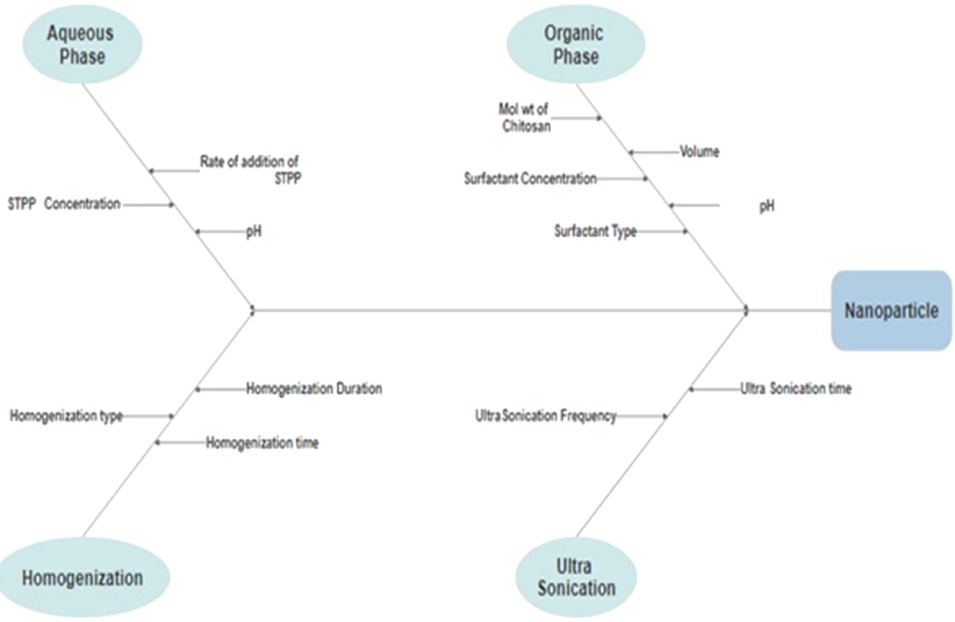

Figure 1. Fishbone diagram for SB-loaded chitosan nanoparticle formulation.

the sample in deionized water, with a 3 month sampling interval.[52,53]

RESULTS AND DISCUSSION

Risk assessment, an aspect of the QbD approach, was introduced to provide the CQAs with a comprehensive insight into critical material attributes and critical process parameters based on the few preliminary literature studies and reviews. The optimization of these parameters could lead to robust formulation of nanoparticles.

Defining the Quality Target Product Profile and Critical Quality Attributes. In order to achieve the QTPP, a number of patient-centric quality attributes (QAs) were determined, including the drug product's physical characteristics, such as particle size (which is necessary for the formulations to reach the intended site), percent entrapment efficiency (better nanoparticulate drug delivery system), and CDR after 48 h (provides insights into its pattern of sustained release), which are commonly selected as CQAs in studies pertaining to QbD-based nanostructured drug delivery systems.

Risk Assessment: Ishikawa Diagram. In order to determine any potential risk associated with the formulation and process variables on the CQA of nanoparticles of silibinin, an Ishikawa diagram was created, which included average particle size, encapsulation efficiency, and cumulative drug release at 48 h. Eight possible risk factors were identified based on prior information, review literature, and exploratory experiments, and these factors were further tested in experimental designs. A fishbone diagram representing the impact of critical material properties and process parameters on the development of silibinin's nanoparticulate drug delivery technology is presented in Figure 1.

Risk Assessment: Plackett–Burman Design. Plackett–Burman (PB) designs are screening designs that have a large number of variables and a limited number of runs. A total of 12 experimental trials were conducted with five independent variables, and the selected response variables showed a wide range, indicating that the independent variables had significant effects on the selected response parameters. ANOVA was used to analyze the data, and a Pareto chart was used to evaluate the parameter. In the Pareto chart (data not shown), effects above the Bonferroni limit are almost certainly significant; effects above the *t*-value limit may be significant and effects below the *t*-value limit are almost certainly not significant. The Pareto chart in Figure 2 shows that speed had the greatest standardized influence at a 95% confidence interval, while chitosan molecular weight had no effect on mean particle size. The data show that the determination coefficients (R^2) were greater than 0.9, suggesting that the model could explain over 90% of the variation in the response and that the model's goodness of fit was validated (data not shown). The obtained *F* value was compared to the theoretical value in order to determine the regression model's relevance. The theoretical value *F* is 7.25. For each regression model, the *F*-ratio was found to be significantly bigger than the theoretical value with a very low probability ($p < 0.001$), indicating that the regression model is significant with a 95% confidence level. The importance of *F* and R^2 indicated that the predicted and observed values were linearly related.[54]

The results from the Pareto chart indicate that as the concentration of chitosan increased, particle size increased, whereas with the increase in STTP concentration and homogenization speed, particle size decreased. Particle size was found between 210 ± 0.15 and 399 ± 1.01 nm.

Equations 12–14 illustrate the polynomial equation that indicates the correlation between the independent variables and the dependent variable

$$Y_1 = 25.36 + 0.0523X_1 - 0.125X_2 + 0.0254X_3 + 0.0025X_4 - 0.0032X_5 + 0.1584X_6 - 0.856X_7 \quad (12)$$

$$Y_2 = 25.847 - 2.325X_1 + 2.321X_2 + 3.254X_3 - 2.3214X_4 - 1.2547X_5 - 2.3256X_6 + 3.2145X_7 \quad (13)$$

https://doi.org/10.1021/acsomega.3c07954
ACS Omega 2024, 9, 10353–10370

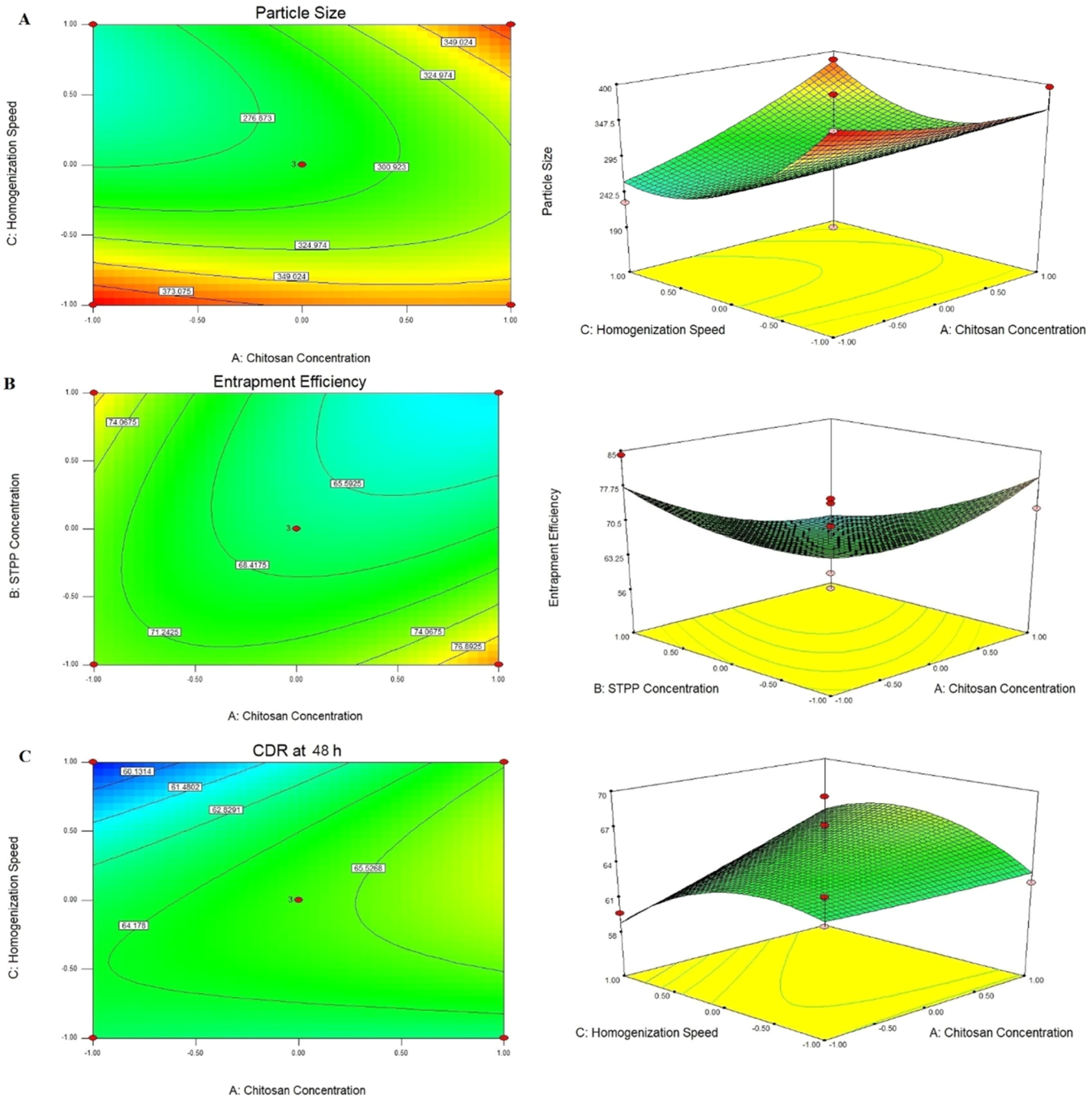

Figure 2. Response surface plot and contour plot for (A) particle size, (B) % entrapment efficiency, and (C) CDR at 48 h.

$$Y_3 = 36.584 + 0.258X_1 + 1.587X_2 - 2.5874X_3 - 3.5874X_4 - 1.8745X_5 + 4.6589X_6 + 5.6547X_7 \quad (14)$$

The coefficients in equations indicate the quantitative impacts of the independent variables on the response variables. When the coefficient has a negative sign, it means that when the value of the independent variable increases, the value of the response variable lowers and vice versa. The absolute value of the coefficient indicates the size of the independent variable and its effect on the response variable; the greater the value, the greater the size. As expected, addition of more chitosan and STPP enhanced EE, whereas an increase in the homogenization speed led to lower EE. The results showed that EE varied between 55.10 ± 0.88 and 79.33 ± 1.23.

Cumulative drug release at 48 h was found from 60.21 ± 1.24 to 72.52 ± 1.69. As the chitosan concentration and STTP concentration increased, cumulative drug release at 48 h was also increased. However, the homogenization speed showed a negative effect on cumulative drug release at 48 h. Placket−Burman design did not evaluate the interaction terms between variables. Hence, still most significant factors were further evaluated by the Box−Behnken design.

Based on the Plackett−Burman design, critical parameters such as chitosan concentration, STTP concentration, and homogenization speed were further studied in the Box−Behnken design.

https://doi.org/10.1021/acsomega.3c07954
ACS Omega 2024, 9, 10353−10370

Optimization by the Box−Behenken Design. *Effect of Independent Variables on Particle Size.* Particle size for all batches lies between 190 ± 0.87 and 398 ± 1.54 nm. In comparison to X_2 and X_3, X_1 had a significant effect on particle size ($p < 0.005$), according to the statistical analysis of particle size data. Particle size was also affected by the interaction terms X_{12} and X_{32}. Having nanoparticles of the ideal size is crucial for both intratumoral distribution and cellular internalization. A smaller size of nanoparticles increases their surface area, which contributes to optimum exposure to the tumorous lung region.[55]

The size of the nanoparticles increased as the chitosan concentration increased. The concentration of the cross-linking agent (STPP) and the homogenization speed on particle size were shown to have an inverse relationship.

The full mode regression eq (eq 15) from effect analysis was obtained for particle size as follows.

$$Y_1 = 214.25 + 32.52X_1 - 12.25X_2 - 32.54X_3 + 25.32X_1X_2 - 32.25X_1X_3 + 6.325X_2X_3 + 65.98{X_1}^2 + 85.25{X_2}^2 + 85.69{X_3}^2 \quad (15)$$

Significant factors were defined as regression coefficients with a p-value less than 0.05. The terms with p-values greater than 0.05 contributed the least to response prediction. As a result, removing nonsignificant ($p > 0.05$) components from the full model and using regression between significant terms gave the reduced model eq 16.[55]

$$Y_1 = 214.25 + 32.52X_1 - 12.25X_2 - 32.54X_3 + 25.32X_1X_2 + 6.325X_2X_3 + 65.98{X_1}^2 + 85.25{X_2}^2 \quad (16)$$

The Fisher F test with probability ($P > F = 0.0231$) demonstrated that the model was significant in ANOVA, showing that selected factors had a substantial effect on particle size. The correlation between independent and dependent variables was investigated using response surface plots.

The result showed that as the chitosan concentration increased, particle size also increased. This mainly occurred due to formation of a more viscous solution as the concentration of chitosan was high.[56] A similar effect of polymer concentration on particle size of nanoparticles was reported by many researchers such as Mainardes and Evangelista[57] and Quintanar-Guerrero et al.[58] In order to decrease chitosan mobility and enhance physical properties like stability, cross-linking compounds are typically used in the formulation of nanoparticles. STPP is a polyanion that interacts with the chitosan amino groups during the ionic gelation process to generate a gel via inter- and intramolecular cross-linkages. The production of CSNPs causes the nanoparticle dispersion to become increasingly turbid as the amount of STPP increases. When the STPP concentration was very low, the reaction solution was clear and viscous, similar to a pure chitosan solution, indicating that the STPP concentration was insufficient to produce a cross-linked structure of chitosan. As the amount of STPP increased, NP began to develop, and particle sizes decreased. This could be owing to enhanced inter- and intracellular cross-linking. This could be because chitosan and STPP improved inter- and intra-cross-linking. However, as the amount of STPP increased to more than 1%, the size of the CSNPs started to increase. This might be the result of more chitosan molecules being involved in the creation of a single nanoparticle due to the excess STPP after the chitosan molecules had fully cross-linked.[59,60] Since the homogenization speed was based on the speed of the rapidly rotating mixing heads, it was an excellent measure of the energy input to the system. The mechanical collision with the wall caused by the high acceleration of the liquid and the shear stress in the space between the rotor and the stator due to the rapid rotation of the stator were the mixing forces that broke the larger droplets into smaller ones. Homogenization at high speeds reduces particle size, allowing the synthesis of smaller nanoparticles. More energy is produced in the process as the homogenization speed increases, resulting in rapid dispersion of the polymeric organic phase and the formation of nanoparticles of small size with a monomodal distribution. Because the mixing energy was insufficient at lower mixing speeds, the final mean particle size of the generated nanodispersions was greater in this operational area. Lower homogenization speeds resulted in a bimodal distribution, which could be attributed to insufficient organic-phase dispersion. However, at 15,000 rpm, the process was difficult to manage in terms of froth and air bubble formation. The response surface plot and the contour plot for particle size are shown in Figure 2A.

Effect of Independent Variables on Entrapment Efficiency. Entrapment efficiency for all batches lies between 56.16 ± 0.98 and 81.21 ± 0.98%. From the statistical analysis of entrapment efficiency data, it can be observed that X_1 and X_2 had significant effects on entrapment efficiency as compared to X_3. Interaction terms X_{12} and X_{13} also had significant effects on entrapment efficiency.

The full mode and reduced model regression equations from effect analysis were obtained for entrapment efficiency as below eqs 17 and 18.

$$Y_2 = 325.52 + 26.58X_1 + 18.95X_2 - 25.54X_3 + 35.65X_1X_2 - 87.54X_1X_3 + 15.254X_2X_3 + 78.56{X_1}^2 + 89.65{X_2}^2 - 82.65{X_3}^2 \quad (17)$$

$$Y_2 = 325.52 + 26.58X_1 + 18.95X_2 + 35.65X_1X_2 - 87.54X_1X_3 + 78.56{X_1}^2 + 89.65{X_2}^2 \quad (18)$$

The Fisher F test with probability ($P > F = 0.0158$) in ANOVA demonstrated that the model was significant, showing that selected variables had a substantial effect on EE. The correlation between independent and dependent variables was investigated using response surface plots. Drug entrapment efficiency (%) (Y_2) improved with increasing chitosan concentration, owing to greater bond formation between drugs and the polymer. Furthermore, a higher amount of chitosan has a better capacity for ionic gel formation, which inhibits silibinin from moving to the external phase and boosts drug encapsulation efficiency. The increase in viscosity of the organic phase (emulsion droplet) of the W/O/W emulsion between the two aqueous phases (internal drug solution and external surfactant solution) can explain the increase in DEE with the polymer concentration. This increase in the viscosity of the organic phase can reduce drug diffusion from the internal aqueous phase to the external. As a result, more drug molecules are incorporated into the nanoparticles, which improves DEE. Mao and colleagues reported a 2-fold increase in DEE as polymer content increased (from 8 to 32%).[61] With an increase in STPP concentration, the chitosan matrix's cross-

https://doi.org/10.1021/acsomega.3c07954
ACS Omega 2024, 9, 10353−10370

linking density improves, resulting in increased entrapment efficiency.[61] When the emulsification speed was increased from 5000 to 15,000 rpm, the encapsulation efficiency increased from 65.21 to 84.12%. Although not linear, increasing the homogenization speed from 10,000 to 15,000 rpm (69.52 to 77.62%) enhanced the encapsulation efficiency more than increasing the homogenization speed from 5000 to 10,000 rpm (65.21 to 70.32%). A unidirectional and less turbulent flow in the case of a lower speed may have contributed to the drug loss from the organic phase, which could account for the increase in encapsulation efficiency. The response surface plot and the contour plot for encapsulation efficiency are shown in Figure 2B.

Effect of Independent Variables on CDR at 48 h. CDR at 48 h for all batches lies between 59.65 ± 2.14 and 70.54 ± 2.05%. From the statistical analysis of CDR at 48 h, it can be observed that X_1 and X_3 had significant effects on CDR at 48 h as compared to X_2. Interaction terms X_{13} and X_{23} also had significant effects on CDR at 48 h. The full mode and reduced mode regression eqs (eqs 19 and 20) from effect analysis were obtained for CDR at 48 h.

$$Y_3 = 215.32 + 15.62X_1 + 32.58X_2 + 45.32X_3 - 58.65X_1X_2 + 67.85X_1X_3 + 25.89X_2X_3 + 47.58X_1^2 + 86.32X_2^2 - 98.58X_3^2 \quad (19)$$

$$Y_3 = 215.32 + 15.62X_1 + 45.32X_3 + 67.85X_1X_3 + 25.89X_2X_3 + 47.58X_1^2 - 98.58X_3^2 \quad (20)$$

The model was shown to be significant in ANOVA, with a significant effect of chosen variables on particle size, according to the Fisher F test with probability ($P > F = 0.0235$). Using response surface plots, the relationship between independent and dependent variables was explained.

As polymer and cross-linking agent concentration increased, a more cross-linking structure was formed, which took more time to diffuse the drug from the polymer matrix, so it sustained drug release. However, the increasing polymer after a point resulted in a decrease in vitro drug release, which is a trend predicted to decrease the release rate with an increase in polymer density in the matrix. The burst release of nanoparticles might be due to the diffusion of the drug that was adsorbed on the surface of nanoparticles. Drug release was increased with the increase in the rate of addition of chitosan, indicating the better cross-linking density of the chitosan matrix.[62] The response surface plot and the contour plot for CDR at 48 h are shown in Figure 2C.

The total amount of drugs released after 48 h increased as the homogenization speed increased. Due to the high particle size and low yield caused by the slow homogenization speed, the difference in release profiles can be related to the particle size of the nanoparticles. Larger particles showed a slower rate of drug release due to the longer diffusion paths that the drug had to travel to reach the dissolving medium.[63]

Validation of the Model. The BBD overlay plot from Design-Expert software was used to help select the optimal combination of independent factors to formulate NPs. From point prediction software, one formulation was chosen for Design-Expert, and its responses were evaluated. Based on the predetermined values of the dependent variables, the optimization technique yielded the expected results. To confirm the accuracy of the optimized formulation, the experimental values (actual) of a selected batch are compared to the predicted values of dependent variables. Checkpoint batches were obtained from an extensive grid search. Based on the overlay plot, checkpoint batch CP_1 was formulated using a chitosan concentration of 1.73%, an STPP concentration of 0.91%, and a homogenization speed of 12,500 rpm, having a predicted particle size of 273 nm, an entrapment efficiency of 76.55%, and the CDR at 48 h of 62.82%. The experimental particle size is 275 ± 1.20 nm, the entrapment efficiency is 75.52 ± 0.87%, and the CDR at 48 h is 63.25 ± 1.21%, respectively, which shows an error of less than 8% in all responses.

Physicochemical Characteristics. The PDI values for all batches fall between 0.125 ± 0.08 and 0.879 ± 0.112. To achieve a uniform size distribution in the formulations, a smaller PDI value is highly desirable. The presence of positively charged chitosan in nanoparticles results in a positive ζ-potential of larger than 30 mV, indicating exceptional colloidal stability. If chitosan concentration increases from lower to high, the ζ-potential increases because of the presence of a cationic amino group in the chitosan.[64,65] ζ-Potential decreased with an increase in STPP concentration. STPP is anionic in nature, so the presence of a higher amount of STPP on the surface of nanoparticles could decrease the ζ-potential (31.50 ± 0.25 to 39.89 ± 0.41 mv).

Release Kinetics and Mechanisms of Drug Release. The release effect shows that the drug was released from formulations in the range from 58.45 ± 0.87 to 70.54 ± 2.05% within 48 h. It follows a biphasic release mechanism. For instance, 10−12% of drug release in the first 2 h and 65−70% within 48 h. The drug release mechanism from CSNPs is related to the amount of drug on the particle surface, drug diffusion from the CS matrix, and CS degradation and erosion. The presence of free SB in the external phase and on the nanoparticle surfaces could have caused the burst release. Due to the solid matrix of NPs and the resulting immobilization of the drug, a gradual and sustained release profile is expected.[66,67] Furthermore, chitosan interacts with biological fluids, salts, and various delivery media to which formulations are exposed, allowing for even more precise drug release control. To summarize, the initial burst release revealed that drugs may be attached to nanoparticles near the particle surface and release when they come into contact with the dissolution medium. Increased diffusion allows the drug to be released for a longer period of time. The polymeric shell surrounding it has a distance and obstructive impact on it.

Several mathematical models were used to investigate the release kinetics and mechanisms of silibinin from CSNPs in this study (zero order, first order, Higuchi, Hixson−Crowell and Korsmeyer−Peppas). The exponent n (correlation values) of the release data that well fitted to the Korsmeyer−Peppas release model is approximately 0.3, confirming that Fick diffusion is the controlling factor for drug release according to the correlation values. The data from drug release kinetics suggest that drug release from nanoparticles may follow a complex mechanism of diffusion and erosion, as best supported by the Korsmeyer−Peppas kinetic model. Furthermore, formulations suit the Korshmeyer−Peppas model well (0.748). In this case, anomalous SB diffusion from NPs is demonstrated by "n" values ranging from 0.43 to 0.85, where drug release is regulated by NP erosion and polymer chain relaxation.[68]

https://doi.org/10.1021/acsomega.3c07954
ACS Omega 2024, 9, 10353−10370

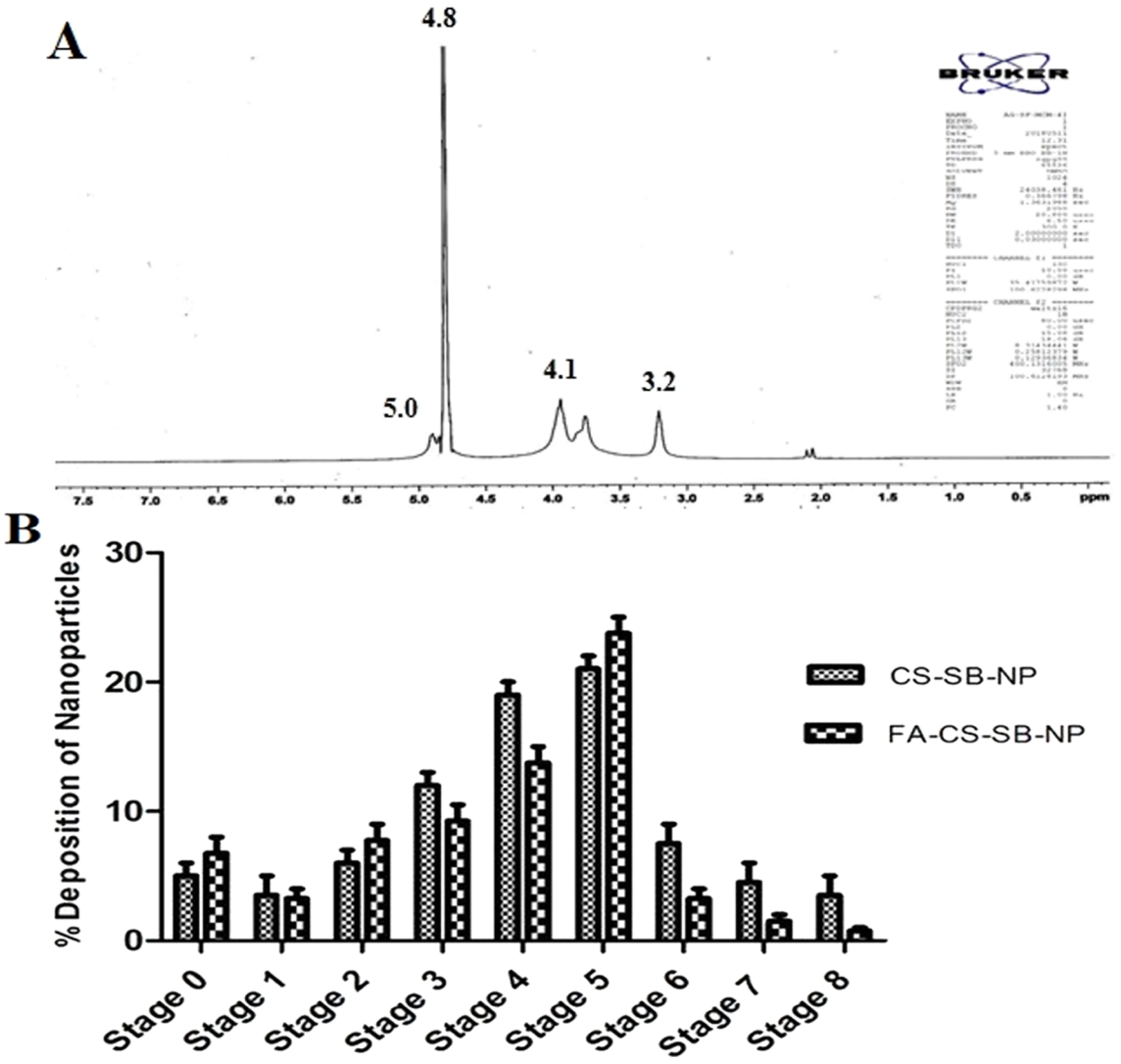

Figure 3. (A) NMR spectrum of FA-CS-SB-NPs and (B) aerosolization behavior of CS-SB-NP and FA-CS-SB-NPs from the Anderson cascade impactor.

Folic Acid Conjugation. Folic acid was successfully conjugated to a batch of CS-SB-NP that had been optimized. The *Z*-average of the uncoated nanoparticles (226 ± 1.05 nm) and the coated nanoparticles (277 ± 1.15 nm) with chitosan was both significantly smaller than 300 nm. It has been discovered that the obtained particle size range is distributed throughout the lungs through pulmonary administration (i.e., from the region of the upper lobe to the lower lobe).[69]

NMR Study. Folic acid conjugation to chitosan was demonstrated using NMR. The presence of two carboxylic groups (−COOH) at the terminal position of folic acid makes it more reactive. The formation of an amide bond between the activated *N*-hydroxysuccinimide ester of folic acid and the primary amine groups of chitosan led to the synthesis of FA-CS-SB-NPs. Figure 3A shows the NMR spectrum of folic acid-conjugated nanoparticles. The acetamino group CH_3 was responsible for the peaks at 3.256 ppm, whereas the carbons 3, 4, 5, and 6 of the glucosamine ring of chitosan were responsible for the CH peak at 4.125 ppm. The formation of an amide bond between the activated folic acid ester and the primary amine groups of chitosan gave strange signals at approximately 5.680 ppm, corresponding to the H22 folic acid proton.[70] Salar et al. acquired similar findings by grafting folic acid on chitosan for silibinin delivery to specific targets.[71,72]

Formulation of a Dry Powder Inhaler and Characterization. Formulations were combined using the geometrical dilution method with anhydrous inhalable-grade lactose at a ratio of 1:1:05 in order to improve the flow property and convert the FA-CS-SB-NP formulations into an inhalation form. As flow characteristics, the angle of repose, Hausner ratio, and Carr's index were ascertained.

Determination of MMAD and the Geometric Standard Deviation. The size and shape of particles are the most important factors in determining deposition in different parts of the lungs. Aerodynamic particles with a diameter of 0.5−5 μm can reach the alveoli and small airways.[73] The cascade impactor scenario of the nonconjugated and folic acid-conjugated nanoparticles is shown in Figure 3B. Less than 10% of the particles were deposited in phases 0−2 and 6−7. Particle deposition was greater than 10% but less than 20% in stages 3 and 4 but greater than 20% in stage 5. A fine fraction was defined as particle size less than 5.[74] The fine particle fraction, extra fine particle fraction, and emitted dose for unconjugated nanoparticles and folic acid-conjugated nano-

https://doi.org/10.1021/acsomega.3c07954
ACS Omega 2024, 9, 10353−10370

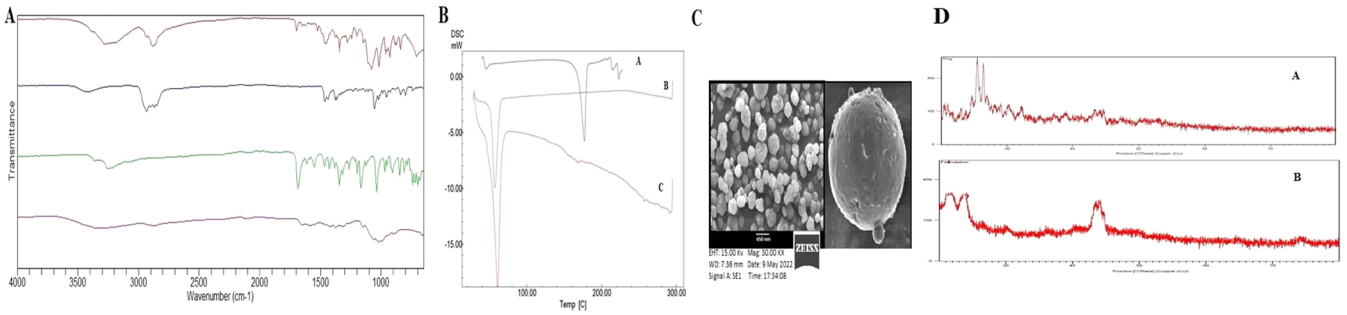

Figure 4. (A) FTIR spectra of (a) silibinin, (b) chitosan, (c) CS-SB-NPs, and (d) FA-CS-SB-NPs. (B) DSC spectra of (a) silibinin, (b) CS-SB-NPs, and (c) FA-CS-SB-NPs. (C) Scanning electron microscopy images of the optimized batch (FA-CS-SB-NPs) for surface study. (D) XRD of a (a) pure drug and (b) optimized formulation (FA-CS-SB-NPs).

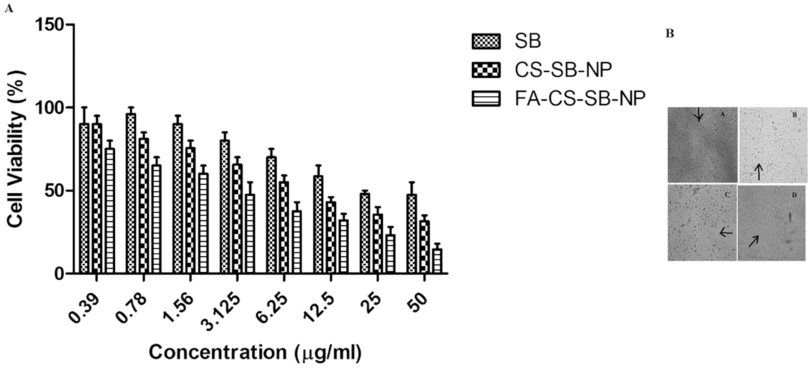

Figure 5. (A) In vitro cytotoxicity analysis of SB, CS-SB-NPs, and FA-CS-SB-NPs in A549 cancer cells using MTT assay. (B) Analyzing the morphology of A549 cancer cells post-treatment with (a) control, (b) SB, (c) CS-SB-NPs, and (d) FA-CS-SB-NPs.

particles were 84.2, 25.68, and 12.5% and 67.8, 21.45, and 8.57% respectively. MMAD and GSD of unconjugated nanoparticles and folic acid-conjugated nanoparticles were calculated to be 2.78 ± 0.85 and 2.10 ± 0.77 μm, as well as 2.75 ± 1.02 and 3.15 ± 0.88 μm, respectively. Dynamic particle size for folic acid-conjugated nanoparticles was 1.74 ± 1.10 μm, and the geometric standard deviation was 1.84 ± 0.98 μm. This shows that the prepared formulation has a deep lung penetration rate. Effective delivery may be facilitated by a tight size distribution centered on fine particle size, as indicated by a low MMAD and low GSD. This indicates that the MDI is capable of reaching the lungs deeply. Based on data collected during particle deposition on various stages of the cascade impactor, the particle size obtained in both formulations (150−400 nm) is relevant for deposition in the trachea, primary and secondary bronchi, and alveolar region for deep lung penetration.[75]

Characterization of the Prepared Formulation. *FTIR Spectroscopy.* Figure 4A displays the FTIR spectra of the drug, polymer, and formulation. The peak at 1031.25 cm^{-1} in the pure chitosan spectrum was attributed to the presence of the saccharide structure. Stretching vibrations of amide I, amide III, and OH were assigned to peaks at 3450.25, 1375.34, and 1582.12 cm^{-1}, respectively. The FTIR spectra of silibinin showed peaks at 1434.14, 3376.44, and 1663.04 cm^{-1}, corresponding to the symmetric aromatic ring stretching vibration (C═C ring), phenolic (OH) vibrations, and mixed (C═O) amide and (C═C) vibrations, respectively. CSNPs loaded with silibinin demonstrated C═C aromatic, N−H/C−H stretching, and CH_2 wagging associated with the OH groups of chitosan at 1549.35 and 1482.20 cm^{-1}.[76] When the folate-modified chitosan was compared to the chitosan spectra, a new amide bond, indicating the IR band, was found at 1560 cm^{-1}. As shown in Figure 4A, the absence of the drug's characteristic peak indicates that the drug was successfully entrapped within the polymeric matrix of the nanoparticles. This led to the conclusion that the drug and polymer were compatible with one another and did not interact.

DSC. The DSC thermogram of pure silibinin shows a broad endothermic peak at 146.19 °C, corresponding to its melting point. The DSC thermogram of CS-SB-NP and FA-CS-SB-NP showed an endothermic peak between 82.48 and 84.34 °C and an exothermic peak between 190.25 and 192.68 °C of chitosan, as indicated in Figure 4B. The endothermic peak, also known as the dehydration temperature (TD), is attributed to water loss associated with chitosan's hydrophilic groups. The total removal of the distinctive peak of silibinin in the DSC thermogram of nanoparticulate formulation indicates that the medication was molecularly dispersed within the polymeric matrix.[77] The DSC curve of silibinin, CS-SB-NPs, and FA-CS-SB-NPs is shown in Figure 4B.

Scanning Electron Microscopy Study. Using scanning electron microscopy, the optimized batch (FA-CS-SB-NPs) morphology was investigated. The SEM study images are displayed in Figure 4C. The scanning electron microscopy (SEM) images of the folic acid-conjugated silibinin-loaded nanoparticles revealed a smooth surface and a spherical shape.

X-ray Diffraction. From the XRD studies, silibinin (Figure 4D) shows diffraction peaks at 2θ of 17.75, 19.31, 23.5, 26.15, and 28.19°. Some of the peaks are sharp and strong, indicating that silibinin in its natural state is crystalline. The prepared FA-CS-SB-NPs show diffraction peaks in the same range with roughly half the intensity, indicating that the crystalline nature has been reduced to the amorphous form.[78] These results

https://doi.org/10.1021/acsomega.3c07954
ACS Omega 2024, 9, 10353−10370

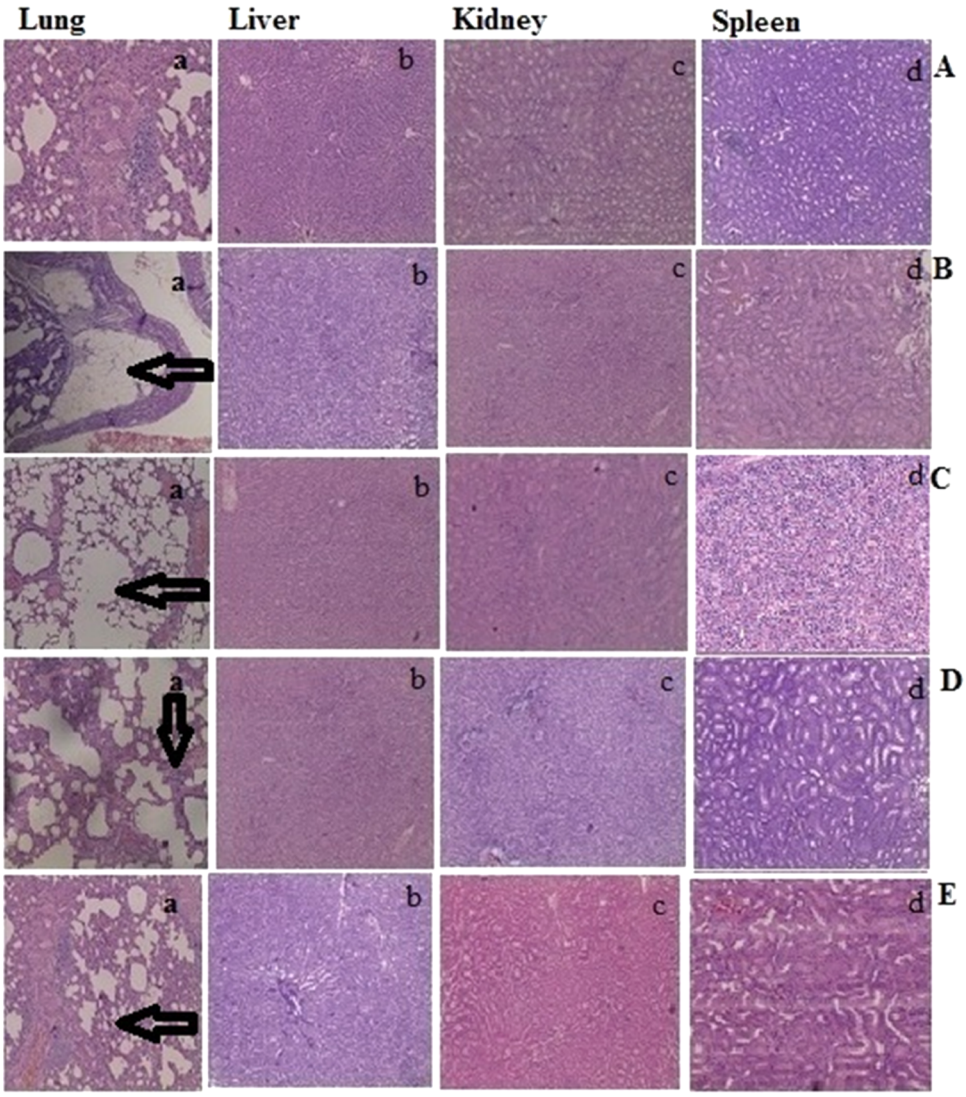

Figure 6. Microscopic images illustrating pathological alterations in different organs. (A) Control group, (B) group treated with NNK after 3 months, (C) group treated with NNK after 5 months, (D) treatment with CS-SB-NP formulation after the 2nd month, and (E) treatment with FA-CS-SB-NP formulation after the 2nd month.

indicate that silibinin was successfully encapsulated into the nanoparticles as a molecular dispersion. Some reflections can be observed, indicating the semicrystalline nature of folic acid. Figure 4D shows several sharp reflections at 2θ of 45.2 and 47.5°, indicating the reflection pattern of folic acid, thus indicating that the conjugation of folic acid in the chitosan drug matrix was accomplished.

In Vitro Cytotoxicity Assay. The capacity of nanoparticles to enter into cancer tissues and cells is the most critical requirement for their pharmacological effectiveness, as this ensures that the drug is available for a long time. Therefore, lung cells were subjected to a cellular uptake assay.

MTT assay was used to assess cell viability after exposing the A549 cell line to various concentrations of free SB, CS-SB-NPs, and FA-CS-SB-NPs (0.39−50 g/mL) for 24 h at 37 °C. Figure 5A shows that the cellular absorption efficiencies of both CS-SB-NPs and FA-CS-SB-NPs in A549 cells are concentration-dependent. However, FA-CS-SB-NPs had a substantially higher uptake efficiency than CS-SB-NPs. Folic acid receptor-targeted FA-CS-SB-NPs showed significantly ($p < 0.05$) better cellular uptake in A549 cancer cells than nontargeted formulations. Again, the availability of FA on the particle surface, which may facilitate ligand−receptor interactions and is abundant in A549 cells, might increase the drug concentration inside the intracellular environment, which is the primary reason for FA-CS-SB-NPs' uptake in most cases. To determine the true cytotoxic effect of formulations on cancer cells, the IC50 value was used. It is the concentration required to kill 50% of the initial cells. After 24 h of incubation with FA-CS-SB-NPs, the IC50 value was found to be 24.5 g/mL. Nanoparticles have been shown to minimize the MDR effect, which should boost SB's anticancer potency by lowering the P-glycoprotein-mediated efflux from cells. The significant cellular absorption of FA-CS-SB-NPs in A549 cancer cells is consistent with its enhanced anticancer impact.

Microscopic Analysis. After treatment with anticancer drugs, a morphological study of cancer cells was performed. The formulations were incubated for 24 h after being exposed to cancer cells. The control cells were normal and spread over the well plate coverslip, but cells in the formulation-treated group shriveled. The morphology of cancer cells differed between formulations, which was consistent with the

https://doi.org/10.1021/acsomega.3c07954
ACS Omega 2024, 9, 10353−10370

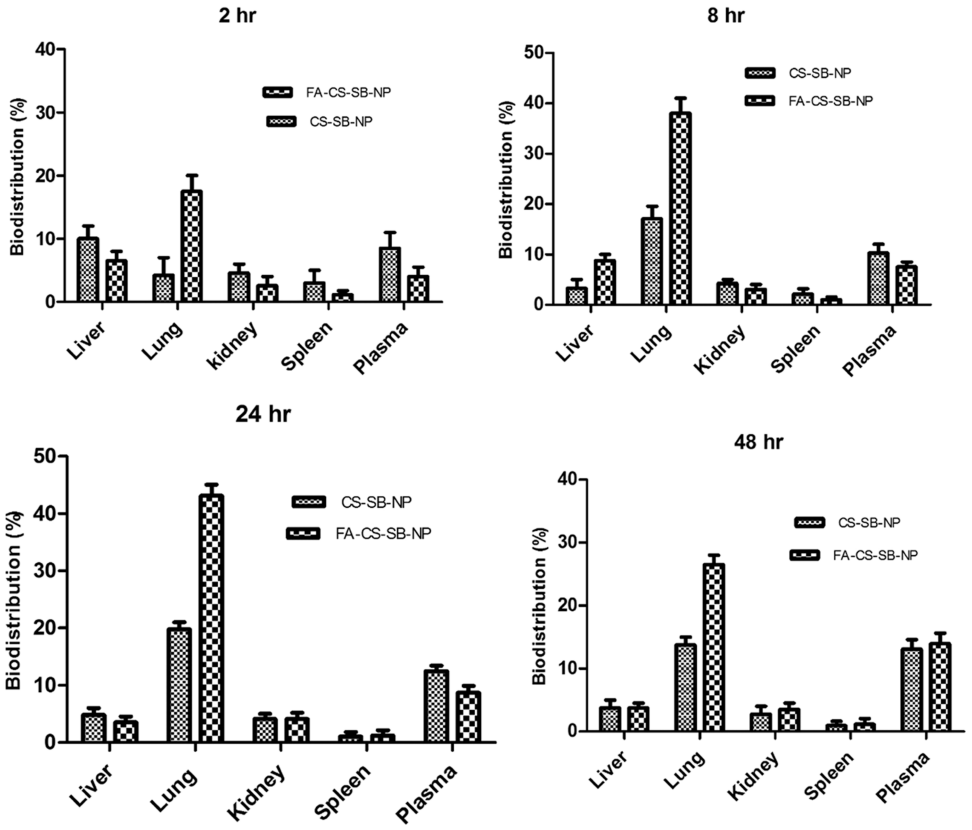

Figure 7. Biodistribution study of CS-SB-NP and FA-CS-SB-NP formulations in various organs (liver, lungs, kidneys, spleen, and plasma) at 2, 8, 24, 48 h.

cytotoxicity experiment. FA-CS-SB-NP-treated cells had fewer and rounder morphologies, indicating that the formulations were more cytotoxic. Because of its somewhat increased absorption in cancer cells, the SB also caused significant alterations in cancer cells. These findings clearly show that folic acid-linked nanoparticles will be effective in the treatment of lung cancer (Figure 5B).

In Vivo Study. *NNK-Induced Lung Cancer Model. Biochemical parameters. **Lipid Peroxidation***: The MDA concentration was used as an indication to detect changes in lipid peroxidation levels in sera. When compared to the control group, the MDA content in the sera of NNK-treated rats increased significantly by 4.21, 21.4, and 35.16% at 2, 3, and 4 months, respectively (data are not shown).

Activity of Superoxide Dismutase and Catalase. During the progression of the disease, the levels of enzymatic antioxidants in the sera of control and treated rats were compared. When compared to the control group, SOD activities in the NNK treatment group were reduced by 10.437, 29.16, and 45.21% at 2, 3, and 4 months, respectively (data are not shown). Catalase activity in the diseased group decreased significantly with time by 5.21, 12.3, 19.6, and 23.56%, respectively (data are not shown).

Reduced Glutathione Level. The effect of NNK on serum levels of the nonenzymatic antioxidant GSH. When compared to the control group, the NNK-treated group exhibited a significant decline of 5.21, 10.23, and 19.85% at various time intervals (data are not shown).

In experimental animals, exposure to NNK has been linked to the development of neoplastic tumors.[79] It is feasible to acquire a better understanding of the mechanisms underlying the changed metabolic process in human lung cancer by investigating biochemical abnormalities in an animal model. NNK, on the other hand, has been shown to disrupt the mitochondrial respiratory chain, resulting in an increase in the superoxide anion and hydrogen peroxide generation. Due to the disruption of cellular functions and integrity, this may result in increased lipid peroxidation and oxidatively damaged macromolecules, such as lipids, DNA, RNA, and antioxidant enzymes, in subsequent cells.[80]

Histopathological Observation. Figure 6A provides an illustration of the histology of a control network in these types of tissues. The test group animals in the 3rd month (Figure 6B) showed atypical changes in the bronchial epithelial lining, an in the 5th month showed tumor cells in alveolar septa (Figure 6C). However, tumors treated with CS-SB-NPs (Figure 6D) had missing extracellular networks, indicating superficial activity on lung cancer tumors. Tumors treated with FA-CS-SB- NPs (Figure 6E) demonstrated that folate receptor levels were maximal in groups receiving FA-CS-SB-NP nanoparticulate formulations compared to the control group. The expression of folate receptors in comparison to the standard group suggests potentially outstanding results in terms of the treatment of lung malignancies. It can be inferred that FA-CS-SB-NPs' increased tumor-specific activity was caused by their targeting of FR, which is overexpressed in lung cancer tumors. Histopathological examinations revealed no alterations in the treated group's other organs, including the liver, spleen, and kidneys. All of the preceding findings show that FA-CS-SB- NPs have improved toleration, selectivity, and therapy efficacy in A549 lung cancer. FA-CS-SB- NPs are a

https://doi.org/10.1021/acsomega.3c07954
ACS Omega 2024, 9, 10353−10370

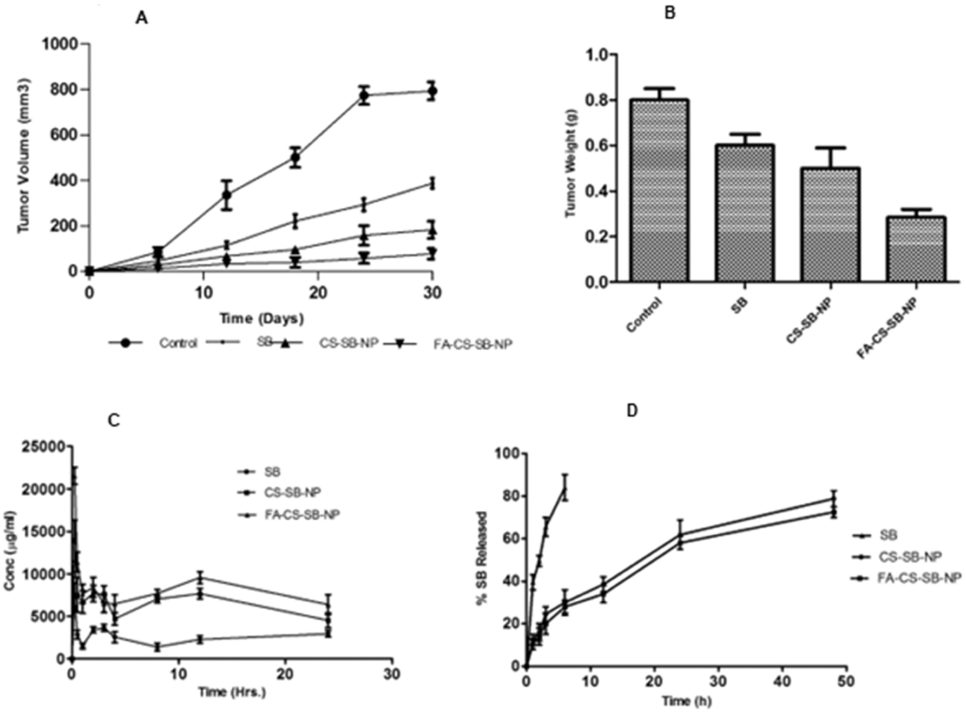

Figure 8. (A) Alterations in the rat tumor volume following the administration of saline, SB, CS-SB-NPs, and FA-CS-SB-NPs. (B) Assessing mice tumor weights following a 30-day treatment period. (C) Plasma kinetics of nanoparticles (CS-SB-NPs and FA-CS-SB-NPs) in the rat. (D) Lung kinetics of nanoparticles (CS-SB-NPs and FA-CS-SB-NPs) in the rat after inhalation administration of nanoparticles.

Table 1. Pharmacokinetic Parameters of Silibinin Solution, Chitosan NPs, and Folic Acid-Conjugated Chitosan NPs in the Plasma and Lung Kinetics in the Sprague-Dawley Rats[a]

	plasma kinetics			lung kinetics		
parameters	silibinin solution	CSNPs	folic acid-conjugated NPs	silibinin solution	CSNPs	folic acid-conjugated NPs
C_{max} (μg/mL)	23.62 ± 13.25	45.25 ± 11.25	102.3 ± 28.02	32.45 ± 25.85	68.58 ± 58.54	25832.12 ± 42.12
T_{max}	1 ± 2.21	4 ± 1.25	3 ± 3.21	1 ± 2.21	12	14
AUC_{total} (μg h/mL)	978.5 ± 118.52	1253 ± 84.58	2588.62 ± 256.31	745.2 ± 102.5	1587.22 ± 247.25	4958.55 ± 325.5
$T_{1/2}$ (h)	8.9 ± 1.25	11.25 ± 2.25	16.4 ± 5.21	4.3 ± 0.58	45.85 ± 1.89	56.32 ± 3.65
CL (1/h)	0.87 ± 0.89	0.78 ± 1.22	0.62 ± 2.58	0.57 ± 1.02	0.52 ± 0.85	0.48 ± 1.02
MRT (h)	4.25 ± 1.05	4.85 ± 2.21	9.58 ± 1.25	3.88 ± 0.87	5.65 ± 0.88	8.54 ± 1.76
F_{rel}	1	3.18	5.20	1	4.21	8.20

[a]Results are in triplicate (n = 3).

good choice because of their high drug loading, ease of production, and quick cellular uptake.

Tissue Distribution Study. The administration of SB by CS-SB-NPs and FA-CS-SB-NPs determined the drug's sustainability and extended residence time in several deep-seated organs (Figure 7). When CS-SB-NP and FA-CS-SB-NP formulations were administered, the highest concentration of SB was found in the lungs, followed by the liver and kidneys. The drug was localized in the lung tissue at 20.96 ± 2.23 and 41.25 ± 3.25% for CS-SB-NPs and FA-CS-SB-NPs, respectively, after 48 h.

These findings suggest that formed surface-engineered NPs have a higher targeting efficiency. The drug concentration in the liver and kidneys is much lower, and the spleen is nearly nonexistent. Thus, there is no risk of cell toxicity. Our findings reveal that FA-CS-SB-NPs allowed for more drug accumulation in the lung tissue than in nontargeted organs (Figure 7). According to the findings, FA plays an important role in the selective localization of FA-CS-SB-NPs in lung cancer cells. The folic acid receptors identified the FA-anchored nanoparticles, which were then delivered to lung malignant cells via receptor-mediated endocytosis. In comparison to folic acid-conjugated nanoparticles, unconjugated CSNPs accumulate in the lungs in smaller amounts.

In Vivo Antitumor Activity. Figure 8 shows the antitumor activity of plain SB, CS-SB-NPs, and FA-CS-SB-NPs. The free medication did not diminish the tumor volume. It is most likely due to its quick elimination from circulation or its decreased tumor-targeting efficacy. However, free medication did appear to slow the rapid development in the tumor volume, as evidenced by the steady climb in the curve of the animals administered with normal saline. SB-loaded CSNPs were found to reduce the tumor volume. Interestingly, from the 2nd day onward, the free drugs demonstrated enhanced and considerably stronger (p0.001) antitumor efficacy than SB administered by CS-SB-NPs and FA-CS-SB-NPs. The larger tumor volume reduction was estimated with FA-CS-SB-NPs (Figure 8A). This is because folic acid-conjugated FA-CS-SB-NPs are actively targeted to overexpressed FA receptors on tumor surfaces. It also resulted in higher NP uptake than with

https://doi.org/10.1021/acsomega.3c07954
ACS Omega 2024, 9, 10353−10370

unconjugated NPs. This could be a characteristic of FA-CS-SB-NPs' specific accumulation in tumors followed by receptor-mediated endocytosis, resulting in better antitumor action when compared to CS-SB-NPs. The tumor weight of the FA-CS-SB-NP group also demonstrated good anticancer activity, as indicated in Figure 8B. In vivo, antitumor effectiveness results suggested that FA-CS-SB-NPs could be helpful in the treatment of lung cancer.

Pharmacokinetic Study. After a single dosage of silibinin-containing nanoparticles was administered via the pulmonary route, the levels of silibinin in the blood and lungs were measured. Various pharmacokinetic parameters after pulmonary administration of free silibinin, CS-SB-NPs, and FA-CS-SB-NPs are listed in Table 1.

The drug level was measured at six distinct time intervals ranging from 6 to 48 h (Figure 8C). In comparison to free silibinin, both nanoparticles demonstrated sustained drug release profiles for up to 48 h (Figure 8D). Our formulation demonstrated the ability to keep the plasma concentration of silibinin above the minimum inhibitory concentration (0.5 mg/L) required for effective lung cancer treatment. When compared to the silibinin solution, the maximum plasma concentration (C_{max}) achieved was nearly four times greater for manufactured folic acid-attached nanoparticles, and the time to achieve maximum plasma concentration was reduced from 3 to 1 h. However, it was discovered that the free drug reached its peak in the lungs and plasma in just 1 h. This finding suggests that administering prepared nanoparticles will increase the rate of absorption. Every time point showed that the prepared nanoparticles' plasma concentration was noticeably higher than that of the ones administered with the silibinin solution. Folic acid-conjugated nanoparticle formulation increased the AUC 3.45 times and 7.25 times in plasma and lungs, respectively. The improved AUC values suggest that the drug availability of the formulation was higher for the folic acid-conjugated nanoparticle formulation. The improved bioavailability of silibinin after pulmonary administration of folic acid-conjugated nanoparticles can be attributed to several reasons. Folic acid acts as an active targeting agent, directly reaching the targeted site. The difference in serum drug concentrations found resulting from CS-SB-NP and FA-CS-SB-NP therapy is strongly related to surface attributes, selectivity, and conferred various shielding effects.[81]

Toxicity Testing. Table 2 presents the outcomes concerning the immune organ index and weight gain among the three rat groups. The weight gains of rats in the FA-CS-SB-NP group, SB, and control group were 30.21 ±. 25, 29.85 ± 3.21, and 25.45 ± 0.89 g, respectively. According to the foregoing findings, rats belonging to the experimental group gained more weight as compared to rats belonging to the control group. As a result, it is conceivable that the original SB and FA-CS-SB-NPs have a minor influence on rat body weight but have no hazardous effect on their organs. No statistically significant variations were observed in the indices of immune organs between the control and experimental cohorts. The data indicate comparable organ metrics in both groups.

Table 2. Effects of FA-CS-SB-NPs on the Different Indices of Rat Immune Organs (Toxicity Level)

group	increment in weight[b] (g)	kidney organ index (mg/g)	lung organ index (mg/g)	spleen organ index (mg/g)	liver organ index (mg/g)
control group	25.45 ± 0.89	3.26	6.20	7.45	38.58
pure SB	29.85 ± 3.21	3.78	6.27	7.42	39.52
folic acid-conjugated CSNPs	30.21 ±. 25	3.29	6.22	7.47	38.87

[b]Results are in triplicate (n = 3).

Stability Study. The study aimed to determine the product's shelf life through accelerated degradation, ensuring a robust estimation. The optimized formulation underwent a 6 month stability study following ICH criteria, assessing particle size, drug entrapment efficiency, and drug release every 48 h (data are not shown). No significant differences were observed in response; hence, formulations were stable. No considerable alterations in particle size (nm), % encapsulation efficiency (% EE), and % cumulative drug release (% CDR) at 48 h were observed at 5 ± 2 °C after 6 months and at 25 ± 2 °C/60 ± 5% RH after 6 months, demonstrating insignificance (p > 0.05). The observed decline in the CDR percentage at the 48 h mark can be attributed to a proportional increase in size coupled with a concomitant reduction in the surface area. The optimized polymeric NP formulations experienced a decline in % EE, attributed to potential silibinin leaching during storage. This decrease in encapsulation efficiency may be a consequence of prolonged storage conditions.[82]

CONCLUSIONS

Silibinin-loaded folic acid-conjugated Inhalation based CSNPs optimized by the QbD approach were developed to treat lung cancer through folate receptor targeting, which is overexpressed in lung cancer cells as compared to free silibinin. Moreover, we found that silibinin-loaded folic acid-conjugated CSNPs maintained a significant silibinin deposition in tissues of the lung tumor along with excellent antiproliferative activity. Additionally, histological research revealed a more effective anticancer effect of nanoparticles on mice lung tumors. The presented results show that silibinin-loaded folic acid-conjugated CSNPs improved therapeutic efficacy and facilitated the targeting of silibinin to tumor sites. This kind of guided drug delivery system demonstrates immense promise for advancing targeted therapies in treating lung cancer, offering enhanced precision and effectiveness.

AUTHOR INFORMATION

Corresponding Authors

Priya Patel − *Department of Pharmaceutical Sciences, Saurashtra University, Rajkot 360005 Gujarat, India*; orcid.org/0000-0001-8572-7169; Email: pvpatel@sauuni.ac.in

Nemat Ali − *Department of Pharmacology and Toxicology, College of Pharmacy, King Saud University, Riyadh 11451, Saudi Arabia*; Email: nali1@ksu.edu.sa

Authors

Mihir Raval − *Department of Pharmaceutical Sciences, Sardar Patel University, Vallabh Vidya Nagar 388120 Gujarat, India*

Vishal Airao − *Department of Pharmaceutical Sciences, Saurashtra University, Rajkot 360005 Gujarat, India*

Gamal A. Shazly − *Department of Pharmaceutics, College of Pharmacy, King Saud University, Riyadh 11451, Saudi Arabia*

https://doi.org/10.1021/acsomega.3c07954
ACS Omega 2024, 9, 10353−10370

Rehan Khan − *Public Health Research Institute (PHRI), Rutgers, New Jersey Medical School (NJMS), Newark, New Jersey 07103, United States*

Bhupendra Prajapati − *Shree S. K. Patel College of Pharmaceutical Education and Research, Ganpat University, Mehsana 384012 Gujarat, India*

Complete contact information is available at: https://pubs.acs.org/10.1021/acsomega.3c07954

Notes

The authors declare no competing financial interest.

■ ACKNOWLEDGMENTS

The authors extend their appreciation to the Deputyship for Research and Innovation, "Ministry of Education" in Saudi Arabia, for funding this research (IFKSUOR3−430-3).

■ REFERENCES

(1) Jemal, A.; Siegel, R.; Ward, E.; et al. Cancer statistics. *Ca-Cancer J. Clin.* **2008**, *58* (2), 71−96.
(2) Yang, J.; Liu, Y. M.; Liu, Y. Z. Advances in the pharmaceutical research on the silymarin. *Nat. Prod. Res. Dev.* **2004**, *16* (2), 185−187.
(3) Kvasnička, F.; Bíba, B.; Ševčík, R.; Voldřich, M.; Krátká, J. Analysis of the active components of silymarin. *J. Chromatogr. A* **2003**, *990* (1−2), 239−245.
(4) Cho, H. J.; Suh, D. S.; Moon, S. H.; et al. Silibinin inhibits tumor growth through downregulation of extracellular signal-regulated kinase and Akt in vitro and in vivo in human ovarian cancer cells. *J. Agric. Food Chem.* **2013**, *61* (17), 4089−4096.
(5) Wang, W.; Chen, T.; Xu, H.; et al. Curcumin-loaded solid lipid nanoparticles enhanced anticancer efficiency in breast cancer. *Molecules* **2018**, *23*, 1578−1582.
(6) Pohlmann, A. R.; Weiss, V.; Mertins, O.; Silveira, N. P.; Guterres, S. S. Spray-dried indomethacin loaded polyester nanocapsules and nanospheres: development, stability evaluation and nanostructure models. *Eur. J. Pharm. Sci.* **2002**, *16*, 305−312.
(7) Duret, C.; Wauthoz, N.; Sebti, T.; Vanderbist, F.; Amighi, K. New inhalation-optimized itraconazole nanoparticle-based dry powders for the treatment of invasive pulmonary aspergillosis. *Int. J. Nanomed.* **2012**, *7*, 5475−5489.
(8) Yao, Q.; Liu, W.; Gou, X. J.; Guo, X. Q.; Yan, J.; Song, Q.; Chen, F. Z.; Zhao, Q.; Chen, C.; Chen, T. Preparation, characterization, and cytotoxicity of various chitosan nanoparticles. *J. Nanomater.* **2013**, *2013*, No. 183871.
(9) Danhier, F.; Vroman, B.; Lecouturier, N.; Crokart, N.; Pourcelle, V.; Freichels, H.; Jérôme, C.; Marchand-Brynaert, J.; Feron, O.; Préat, V. Targeting of tumor endothelium by RGD-grafted PLGA-nanoparticles loaded with paclitaxel. *J. Controlled Release* **2009**, *140*, 166−173.
(10) Shen, Z.; Li, Y.; Kohama, K.; Oneill, B.; Bi, J. Improved drug targeting of cancer cells by utilizing actively targetable folic acid-conjugated albumin nanospheres. *Pharmacol. Res.* **2011**, *63*, 51−58.
(11) Theti, D. S.; Jackman, A. L. The role of α-folate receptor-mediated transport in the antitumor activity of antifolate drugs. *Clin. Cancer Res.* **2004**, *10* (3), 1080−1089.
(12) Chan, P.; Kurisawa, M.; Chung, J. E.; Yang, Y.-Y. Synthesis and characterization of chitosan-g-poly (ethylene glycol)-folate as a non-viral carrier for tumor-targeted gene delivery. *Biomaterials* **2007**, *28* (3), 540−549.
(13) Leamon, C. P.; Reddy, J. A. Folate-targeted chemotherapy. *Adv. Drug Delivery Rev.* **2004**, *56* (8), 1127−1141.
(14) Pilcer, G.; Amighi, K. Formulation strategy and use of excipients in pulmonary drug delivery. *Int. J. Pharm.* **2010**, *392*, 1−19.
(15) Zhang, L. J.; Xing, B.; Wu, J.; Xu, B.; Fang, X. L. Biodistribution in mice and severity of damage in rat lungs following pulmonary delivery of 9-nitrocamptothecin liposomes. *Pulm. Pharmacol. Ther.* **2008**, *21*, 239−246.
(16) Mansour, H. M.; Rhee, Y. S.; Wu, X. Nanomedicine in pulmonary delivery. *Int. J. Nanomed.* **2009**, *4*, 299−319.
(17) Alipour, S.; Montaseri, H.; Tafaghodi, M. Preparation and characterization of biodegradable paclitaxel loaded alginate microparticles for pulmonary delivery. *Colloids Surf., B* **2010**, *81*, 521−529.
(18) Gad, A.; Kydd, J.; Piel, B.; Rai, P. Targeting cancer using polymeric nanoparticle mediated combination chemotherapy. *Int. J. Nanomed. Nanosurg.* **2016**, *2* (3), 1−10.
(19) Doppalapudi, S.; Jain, A.; Domb, A. J.; Khan, W. Biodegradable polymers for targeted delivery of anti-cancer drugs. *Expert Opin. Drug Delivery* **2016**, *13* (6), 891−909.
(20) Ko, J. A.; Park, H. J.; Park, Y. S.; Hwang, S. J.; Park, J. B. Chitosan microparticle preparation for controlled drug release by response surface methodology. *J. Microencapsulation* **2003**, *20*, 791−797.
(21) Bose, A.; Wong, T. W.; Singh, N. Formulation development and optimization of sustained release matrix tablet of Itopride HCl by response surface methodology and its evaluation of release kinetics. *Saudi Pharm. J.* **2013**, *21*, 201−213.
(22) Videira, M.; Almeida, A. J.; Fabra, A. Preclinical evaluation of a pulmonary delivered paclitaxel-loaded lipid nanocarrier antitumor effect. *Nanomedicine* **2012**, *8* (7), 1208−1215.
(23) Tomoda, K.; Ohkoshi, T.; Hirota, K.; Sonavane, G. S.; Nakajima, T.; Terada, H.; Komuro, M.; Kitazato, K.; Makino, K. Preparation and properties of inhalable nanocomposite particles for treatment of lung cancer. *Colloids Surf., B* **2009**, *71* (2), 177−182.
(24) Roa, W. H.; Azarmi, S.; Al-Hallak, M. H.; Finlay, W. H.; Magliocco, A. M.; Löbenberg, R. Inhalable nanoparticles, a non-invasive approach to treat lung cancer in a mouse model. *J. Controlled Release* **2011**, *150* (1), 49−55.
(25) Kawashima, Y.; Handa, T.; Kasai, A.; Takenaka, H.; Lin, S. Y.; Ando, Y. Novel method for the preparation of controlled-release theophylline granules coated with a polyelectrolyte complex of sodium polyphosphatechitosan. *J. Pharm. Sci.* **1985**, *74* (3), 264−268.
(26) Patel, P.; Raval, M.; Manvar, A.; Airao, V.; Bhatt, V.; Shah, P. Lung cancer targeting efficiency of Silibinin loaded Poly Caprolactone /Pluronic F68 Inhalable nanoparticles: In vitro and In vivo study. *PLoS One* **2022**, *17* (5), No. e0267257.
(27) Kushwaha, A. K.; Vuddanda, P. R.; Karunanidhi, P.; Singh, S. K.; Singh, S. Development and Evaluation of Solid Lipid Nanoparticles of Raloxifene Hydrochloride for Enhanced Bioavailability. *BioMed. Res. Int.* **2013**, No. 584549.
(28) Beg, S.; Sandhu, P. S.; Batra, R. S.; Khurana, R. K.; Singh, B. QbD-based systematic development of novel optimized solid self-nanoemulsifying drug delivery systems (SNEDDS) of lovastatin with enhanced biopharmaceutical performance. *Drug Delivery* **2015**, *22* (6), 765−784.
(29) Gidwani, B.; Vyas, A. Preparation, characterization, and optimization of altretamine-loaded solid lipid nanoparticles using Box-Behnken design and response surface methodology. *Artif. Cells, Nanomed., Biotechnol.* **2016**, *44* (2), 571−580.
(30) Zhang, X.; Liu, J.; Qioa, H.; Liu, H.; Ni, J.; et al. Formulation optimization of dihydroartemisinin nanostructured lipid carrier using response surface methodology. *Powder Technol.* **2010**, *197*, 120−128.
(31) Xu, X.; Khan, M. A.; Burgess, D. J. A quality by design (QbD) case study on liposomes containing hydrophilic API: I. Formulation, processing design and risk assessment. *Int. J. Pharm.* **2011**, *419*, 52−59.
(32) Shah, P.; Chavda, K.; Vyas, B.; Patel, S. Formulation development of linagliptin solid lipid nanoparticles for oral bioavailability enhancement: role of P-gp inhibition. *Drug Delivery Transl. Res.* **2021**, *11*, 1166−1185.
(33) Beidokhti, H. R. N.; Ghaffarzadegan, R.; Mirzakhanlouei, S.; et al. Preparation, Characterization, and Optimization of Folic Acid-Chitosan-Methotrexate Core-Shell Nanoparticles by Box-Behnken Design for Tumor-Targeted Drug Delivery. *AAPS PharmSciTech* **2017**, *18*, 115−129.

(34) Korsmeyer, R. W.; Gurny, R.; Doelker, E.; Buri, P.; Peppas, N. A. Mechanisms of solute release from porous hydrophilic polymers. *Int. J. Pharm.* **1983**, *15*, 25−35.
(35) Peppas, N. A. Analysis of Fickian and non-Fickian drug release from polymers. *Pharm. Acta Helv.* **1985**, *60*, 110−111.
(36) Song, H.; Su, C.; Cui, W.; Zhu, B.; Liu, L.; Chen, Z.; Zhao, L. Folic Acid-Chitosan Conjugated Nanoparticles for Improving Tumor-Targeted Drug Delivery. *BioMed. Res. Int.* **2013**, *2013*, No. 723158.
(37) Pilicheva, B.; Katsarov, P.; Kassarova, M. Flowability evaluation of dry powder inhalation formulations intended for nasal delivery of Betahistine Dihydrochloride. *Sikk Manipal Univ. Med. J.* **2014**, *2* (1), 77−90.
(38) Kundawala, A. J.; Patel, V. A.; Patel, H. V.; Choudhary, D. Influence of Formulation Components on Aerosolization Properties ofIsoniazid Loaded Chitosan Microspheres. *Int. J. Pharm. Sci. Drug Res.* **2011**, *3* (4), 297−302.
(39) Patel, P.; Raval, M.; Airao, V.; Bhatt, V.; Shah, P. Silibinin loaded inhalable solid lipid nanoparticles for lung targeting. *J. Microencapsulation* **2022**, *39* (1), 1−24.
(40) Townsend, M. H.; Anderson, M. D.; Weagel, E. G.; Velazquez, E. J.; Weber, K. S.; Robison, R. A.; O'Neill, K. L. Non-small-cell lung cancer cell lines A549 and NCI -H460 express hypoxanthine guanine phosphoribosyl transferase on the plasma membrane. *OncoTargets Ther.* **2017**, *10*, 1921−1932.
(41) Amirsaadat, S.; Pilehvar-Soltanahmadi, Y.; Zarghami, F.; Alipour, S.; Ebrahimnezhad, Z.; Zarghami, N. Silibinin-loaded magnetic nanoparticles inhibit hTERT gene expression and proliferation of lung cancer cells. *Artif. Cells, Nanomed., Biotechnol.* **2017**, *45* (8), 1649−1656.
(42) Bhatnagar, S.; Chaudhary, N.; Katare, D. P.; Jain, S. K. A non-surgical method for induction of lung cancer in Wistar rats using a combination of NNK and high dietary fats. *Protoplasma* **2013**, *250*, 919−929.
(43) Wright, J. R.; Colby, H. D.; Miles, P. R. Cytosolic factors which affect microsomal lipid peroxidation in lung and liver. *Arch. Biochem. Biophys.* **1981**, *206*, 296−304.
(44) Nandi, A.; Chatterjee, I. B. Assay of superoxide dismutase activity in animal tissues. *J. Biosci.* **1988**, *13*, 305−315.
(45) Claiborne, A.; Greenwald, R. A. *Handbook of Methods for Oxygen Radical Research*; CRC Press: Boca Raton, 1985; pp 283−284.
(46) Mohandas, J.; Marshall, J. J.; Duggin, G. G.; Horvath, J. S.; Tiller, D. Low activities of glutathione-related enzymes as factors in the genesis of urinary bladdercancer. *Cancer Res.* **1984**, *44*, 5086−5091.
(47) Rizzardini, M.; Zappone, M.; Villa, P.; et al. Kupffer cell depletion partially prevents hepatic heme oxygenase 1 messenger RNA accumulation in systemic inflammation in mice: role of interleukin 1β. *Hepatology* **1998**, *27* (3), 703−710.
(48) Zou, J.; Su, S.; Chen, Z.; Liang, F.; Zeng, Y.; Cen, W.; Zhang, X.; Yu, X.; Huang, D. Hyaluronic acid-modified selenium nanoparticles for enhancing the therapeutic efficacy of paclitaxel in lung cancer therapy. *Artif. Cells, Nanomed., Biotechnol.* **2019**, *47* (1), 3456−3464.
(49) Paul, P.; Sengupta, S.; Mukherjee, B.; et al. Chitosan-coated nanoparticles enhanced lung pharmacokinetic profile of voriconazole upon pulmonary delivery in mice. *Nanomedicine* **2018**, *13* (5), 501−520.
(50) Wu, M.; Zhong, C.; Deng, Y.; Zhang, Q.; Zhang, X.; Zhao, X. Resveratrol loaded glycyrrhizic acid-conjugated human serum albumin nanoparticles for tail vein injection II: pharmacokinetics, tissue distribution and bioavailability. *Drug Delivery* **2020**, *27* (1), 81−90.
(51) Chalikwar, S. S.; Belgamwar, V. S.; Talele, V. R.; Surana, S. J.; Patil, M. U. Formulation and evaluation of nimodipine-loaded solid lipid nano-particles delivered via lymphatic transport system. *Colloids Surf., B* **2012**, *97*, 109−116.
(52) Guideline ICH. Stability testing of new drug substances and prod-ucts. Q1A (R2), Current Step. 2003.
(53) Alex, M. A.; Chacko, A.; Jose, S.; Souto, E. Lopinavir loaded solid lipid nanoparticles (SLN) for intestinal lymphatic targeting. *Eur. J. Pharm. Sci.* **2011**, *42* (1−2), 11−18.
(54) Kuchekar, A. B.; Pawar, A. P. Screening of factors using Plackett Burman design in the preparation of capecitabine-loaded nano polymeric micelles. *Int. J. Pharm. Pharm. Sci.* **2014**, *6*, 489−496.
(55) Ahmed, T. A.; El-Say, K. M. Development of alginate-reinforced chitosan nanoparticles utilizing W/O nanoemulsification/internal crosslinking technique for transdermal delivery of rabeprazole. *Life Sci.* **2014**, *110* (1), 35−43.
(56) Patel, M.; Sawant, K. A Quality by Design Concept on Lipid Based Nanoformulation Containing Antipsychotic Drug: Screening Design and Optimization using Response Surface Methodology. *J. Nanomed. Nanotechnol.* **2017**, *08*, 442−451.
(57) Mainardes, R. M.; Evangelista, R. C. PLGA nanoparticles containing praziquantel: effect of formulation variables on size distribution. *Int. J. Pharm.* **2005**, *290* (1−2), 137−144.
(58) Quintanar-Guerrero, D.; Fessi, H.; Allemann, E.; Doelker, E. Influence of stabilizing agents and preparatives variables on the formation of poly (D, L-lactic acid) nanoparticles by an emulsification-diffusion technique. *Int. J. Pharm.* **1996**, *143*, 133−141.
(59) Al-nemrawi, N. K.; Alsharif, S.; Dave, R. H. Preparation of chitosan-tpp nanoparticles: The influence of chitosan polymeric properties and formulation variables. *Int. J. Appl. Pharm.* **2018**, *10* (5), 60−65.
(60) Fan, W.; Yan, W.; Xu, Z.; Ni, H. Formation mechanism of monodisperse, low molecular weight chitosan nanoparticles by ionic gelation technique. *Colloids Surf., B* **2012**, *90*, 21−27.
(61) Mao, S.; Xu, J.; Cai, C.; Germershaus, O.; Schaper, A.; Kissel, T. Effect of WOW process parameters on morphology and burst release of FITC-dextran loaded PLGA microspheres. *Int. J. Pharm.* **2007**, *334* (1−2), 137−148.
(62) Paterakis, P. G.; Korakianiti, E. S.; Dallas, P. P.; Rekkas, D. M. Evaluation and simultaneous optimization of some pellets characteristics using a 3^3 factorial design and the desirability function. *Int. J. Pharm.* **2002**, *248* (1−2), 51−60.
(63) Basarkar, A.; Devineni, D.; Palaniappan, R.; Singh, J. Preparation, characterization, cytotoxicity and transfection efficiency of poly(DL-lactide-co-glycolide) and poly(DL-lactic acid) cationic nanoparticles for controlled delivery of plasmid DNA. *Int. J. Pharm.* **2007**, *343* (1−2), 247−254.
(64) Wu, J.; Wang, Y.; Yang, H.; Liu, X.; Lu, Z. Preparation and biological activity studies of resveratrol loaded ionically cross-linked chitosan-TPP nanoparticles. *Carbohydr. Polym.* **2017**, *175*, 170−177.
(65) de Pinho Neves, A. L.; Milioli, C. C.; Müller, L.; Riella, H. G.; Kuhnen, N. C.; Stulzer, H. K. Factorial design as tool in chitosan nanoparticles development by ionic gelation technique. *Colloids Surf., A* **2014**, *445*, 34−39.
(66) Agnihotri, S. A.; Mallikarjuna, N. N.; Aminabhavi, T. M. Recent advances on chitosan-based micro- and nanoparticles in drug delivery. *J. Controlled Release* **2004**, *100*, 5−28.
(67) Ahmed, T. A.; Aljaeid, B. M. Preparation, characterization, and potential application of chitosan, chitosan derivatives, and chitosan metal nanoparticles in pharmaceutical drug delivery. *Drug Des. Dev. Ther.* **2016**, *10*, 483−507.
(68) Atyabi, F.; Saremi, S.; Akhlaghi, S. P.; Dinarvand, R.; Ostad, S. N. Thiolated chitosan nanoparticles for enhancing oral absorption of docetaxel: preparation, in vitro and ex vivo evaluation. *Int. J. Nanomed.* **2011**, *6*, 119−128.
(69) Learoyd, T. P.; Burrows, J. L.; French, E.; Seville, P. C. Chitosan-based spray-dried respirable powders for sustained delivery of terbutaline sulfate. *Eur. J. Pharm. Biopharm.* **2008**, *68*, 224−234.
(70) Lee, D.; Lockey, R.; Mohapatra, S. Folate receptor-mediated cancer cell specific gene delivery using folic acid-conjugated oligochitosans. *J. Nanosci. Nanotechnol.* **2006**, *6*, 2860−2866.
(71) Salar, R. K.; Kumar, N. Synthesis and characterization of vincristine loaded folic acid−chitosan conjugated nanoparticles. *Resour.-Effic. Technol.* **2016**, *2*, 199−214.

https://doi.org/10.1021/acsomega.3c07954
ACS Omega 2024, 9, 10353−10370

(72) Cheng, L.; Ma, H.; Shao, M.; et al. Synthesis of folate chitosan nanoparticles loaded with ligustrazine to target folate receptor positive cancer cells. *Mol. Med. Rep.* **2017**, *16* (2), 1101−1108.
(73) Tena, A. F.; Clara, P. C. Deposition of inhaled particles in the lungs. *Arch. Bronconeumol.* **2012**, *48* (7), 240−246.
(74) Mitchell, J. P.; Roberts, D. L. Current Approaches to APSD Measurements of OIPs Based on Inertial Impaction. In *Good Cascade Impactor Practices, AIM and EDA for Orally Inhaled Products.*; Tougas, T. P.; Mitchell, J. P.; Lyapustina, S. A., Eds.; Springer: MA, USA, 2013; pp 15−55.
(75) Lewis, D.; Copley, M. Inhaled product characterization calculating particle-size distribution metrics. *Pharm. Technol.* **2011**, *11*, 33−37.
(76) Ameya, S.; Vivek, P.; Vandita, K.; Inderbir, S. Formulation and Evaluation of Silymarin-Loaded Chitosan-Montmorilloite Microbeads for the Potential Treatment of Gastric Ulcers. *J. Funct. Biomater.* **2018**, *9*, No. 52.
(77) Cheung, M. K.; Agarwal, M.; Nagar, S.; Nalini, D.; Agarwal, M. K. Chitosan Nanoparticles based Drug Delivery: An Update. *Int. J. Adv. Multidiscip. Res.* **2015**, *2*, 1−13.
(78) Jia, L.-J.; Zhang, D.-R.; Li, Z.-Y.; Feng, F.-F.; Wang, Y.-C.; Dai, W.-T.; Duan, C.-X.; Zhang, Q. Preparation and characterization of silybin-loaded nanostructured lipid carriers. *Drug Delivery* **2010**, *17* (1), 11−18.
(79) Akopyan, G.; Bonavida, B. Understanding tobacco smoke carcinogen NNK and lung tumorigenesis. *Int. J. Oncol.* **2006**, *29*, 745−752.
(80) Chuang, C. H.; Hu, M. L. Synergistic DNA damage and lipid peroxidation in cultured human white blood cells exposed to 4(methyl-nitrosamino)-1-(3-pyridyl)-1-butanone and ultraviolet A. *Environ. Mol. Mutagen.* **2006**, *47*, 73−81.
(81) Lorenz, D.; Lucker, P.; Mennicke, W.; Wetzelsberger, N. Pharmacokinetic studies with silymarin in human serum and bile. *Methods Find. Exp. Clin. Pharmacol.* **1984**, *6*, 655−661.
(82) Helgason, T.; Awad, T. S.; Kristbergsson, K.; et al. Effect of surfactant surface coverage on formation of solid lipid nanoparticles (SLN). *J. Colloid Interface Sci.* **2009**, *334* (1), 75−81.

https://doi.org/10.1021/acsomega.3c07954
ACS Omega 2024, 9, 10353−10370